3-31-2023 12:00 PM

Denoising-Based Domain Adaptation Network for EEG Source Imaging

Runze Li, *The University of Western Ontario*

Supervisor: Boyu, Wang., *The University of Western Ontario*
Co-Supervisor: Charles, Ling., *The University of Western Ontario*
A thesis submitted in partial fulfillment of the requirements for the Master of Science degree in Computer Science

Abstract

Electrophysiological source imaging (ESI) is a widespread and no-invasive technique in neuroscientific research and clinical diagnostics. It provides a well-established and high temporal resolution of source activity and gives the brain signal by analyzing the corresponding EEG signal. However, it is still a major challenge to deal with the domain shift problem between the datasets of different subjects or sessions in ESI problem. Furthermore, the variable noise included in the EEG signals inevitably influence the accuracy of localization of source activity. In this paper, we propose a novel denoising autoencoder-based unsupervised domain adaptation (DAE-UDA) algorithm to tackle these problems. To the best of our knowledge, it is the first to solve the domain shift in the ESI problem by using UDA to narrow the discrepancy between different domains. Moreover, we innovatively combine our model with denoising autoencoder (DAE) to remove noise and learn a robust mapping from the noisy EEG signal to the brain activity. Extensive numerical experiments and the analysis of real EEG datasets demonstrate that DAE-UDA can effectively remove noise and mitigates the domain shift of low-SNR EEG signal. Our model outperforms other classical ESI methods in robustly imaging source activities under a variety of source settings.

Keywords: Electromagnetic source imaging (ESI), Denoising network, Domain Adaptation, Transfer learning, EEG source localization, deep learning

Summary for Lay Audience

In our daily lives, some people suffer from several neurological diseases such as epilepsy, ADHD, Alzheimer's, etc. These neurological diseases may be caused by some lesion areas in patients' brain. Thus, if we could find an effective method to locate the exact localization of the areas of the lesions, many mental illnesses could be alleviated or even cured. Electroencephalogram (EEG) is a recording of brain activity that measures electrical activity in our brain using small metal electrodes attached to the surface of the top of the patient's head. Due to the non-invasiveness and convenience of EEG, some researchers want to measure and analyze patients' EEG signals to find the source in the brain that generates the EEG signal, which may be the location of the brain lesion area. However, there are two main challenges that bother doctors and scientists: the noise in EEG signals impacts the analysis, and the probability distributions of EEG signals and the source of the signal in the brain often change.

In this paper, we propose a new deep learning method call DAE-UDA to solve these problems. Our model mainly consists of two parts: unsupervised domain adaptation and denoising autoencoder. The first component unsupervised domain adaptation technique (UDA) can overcome the change in the distribution of EEG and source activity in the brain and make our model more applicable, and the second component denoising autoencoder (DAE) can remove the noise contained in EEG signals. Extensive numerical experiments and the analysis of real EEG datasets demonstrate that DAE-UDA can effectively remove noise and mitigates the change of distribution of noisy EEG signal.

Acknowledgements

I would like to express my deepest gratitude to my supervisors, Dr. Boyu Wang and Dr. Charles Ling for their constant guidance and support. They not only taught me various skills on how to address academic research questions, but they also provided me with many opportunities to learn, grow, and pursue my interests. It was an absolute honor to work with my supervisors. I would like to express my gratitude to the faculty and staff of the computer science department, especially Janice Wiersma and Ange Muir, for their guidance. In addition, I thank western university for providing me with a generous scholarship that enabled me to conduct this research.

Studying and doing research during the pandemic days, far away from home is a challenging task. I am grateful for all my friends and lab members who helped me to overcome this challenge with their love and support. Especially, I want to thank Jiaqi Li, Pengcheng Xu, Ruizhi Pu and Gezheng Xu.

Most importantly, I am grateful for my family's unconditional, love and support. All my accomplishments and success are because of them. My parents, who always encourage me and support my decisions, deserve special thanks. I owe my deepest gratitude to my mom and dad who taught me to keep faith in what I pursue. To my family, I give everything, including this.

Contents

List of Figures

List of Tables

List of Symbols

$\mathcal{S}$	Source domain
$\mathcal{T}$	Target domain
D_S	Source dataset
D_T	Target dataset
H	Lead field matrix
C^S	Clean EEG signal in source dataset
E^S	Noisy EEG signal in source dataset
E^T	Noisy EEG signal in target dataset
S^S	Source signal in source dataset
S^T	Source signal in target dataset
ε^S	Noise in source dataset
ε^T	Noise in target dataset
G_e	Encoder layer
G_d	Decoder layer
F	Regressor
F_{adv}	Adversarial Regressor
$G_e(E^S)$	Denoising features of source dataset
$G_e(E^T)$	Denoising features of target dataset
L_{re}	Reconstruction loss
L_{UDA}	Unsupervised domain adaptation loss
L_S	Regression loss for samples in source dataset
L_{MDD}	Margin disparity discrepancy loss
λ	Trade-off ratio in L_{re}
$\hat{S}^S$	Regression result of F on source dataset
$\hat{S}^T$	Regression result of F on target dataset
$\hat{S}^S_{adv}$	Regression result of F_{adv} on source dataset
$\hat{S}^T_{adv}$	Regression result of F_{adv} on target dataset

Chapter 1

Introduction

1.1 Introduction

With recent advancements in brain science and bioelectric signal measurement technology, a growing number of medical experts and researchers in the field of brain diseases have discovered that neurological and physiological disorders such as Parkinson's disease, ADHD, and epilepsy are closely associated with brain lesions or abnormal brain electrical signals. As a result, there is a requirement to develop effective methods or algorithms to accurately determine the specific location of brain lesions and the source of abnormal brain electrical signals, whether it is in the brain or the brain stem. This process, known as brain source localization (BSL) or brain source imaging (BSI) problem, involves identifying the position, direction, and depth of the disease source in the brain.

Traditional methods for brain source localization or imaging, such as the subdural electrode method, typically involve invasive techniques that require sensors or electrodes to be inserted into the patient's head and brain in order to record electrical signals from the brain and scalp, with the aim of identifying the location of the disease. However, these invasive methods are associated with drawbacks such as invasiveness, risk of rejection, and potential for causing temporary or permanent damage or dysfunction to the patient's brain, as well as increased susceptibility to infection or edema. As a result, non-invasive methods have been developed in recent years, utilizing physiological signals related to the brain that can be collected from outside the body, such as magnetic resonance imaging (MRI), functional magnetic res-

onance imaging (fMRI), electroencephalogram (EEG), and magnetoencephalography (MEG), among others. Non-invasive techniques offer advantages in terms of safety, cost-effectiveness, non-invasiveness, and patient-friendliness, which have led to significant attention and rapid development in recent years. Among these non-invasive techniques, EEG measurement technology has shown particular promise, with advantages such as high temporal resolution, minimal equipment and measurement environment requirements, and low cost. As a result, EEG has become one of the most widely used biological signals for non-invasive measurement of electromagnetic brain activity [28].

The EEG source imaging problem, also referred to as EEG source localization problem (ESL), is a non-invasive brain source imaging (BSI) problem that aims to reconstruct the high temporal resolution of source activity in the brain using measurements of EEG signals. Among the non-invasive source localization methods, EEG-based brain source localization methods for patients with brain diseases have become widely used for BSI. However, ESI faces challenges due to the poor spatial resolution of EEG signals, resulting in an ill-posed problem. This is caused by the low spatial resolution and limited number of recording sensors compared to the numerous potential source solutions in the brain. In some cases, different source activities in the cortex can result in the same EEG topology recorded on the scalp of patients.

To find the source resolution of EEG signals, statistical ESI methods rely on the optimization or probabilistic framework, where regularization techniques or pieces of prior information about the head conditions of the patient are exploited to constrain the solution space and remove noise for a specific signal-to-noise ratio, such as weighted MNE [15], LORETA [46], and sLORETA [48], etc. However, no matter what strategies are used, these classical ESI methods are unstable owing to noise sensitivities, initial source configurations and also rely on the estimation of the patient's brain physiological properties [5, 18, 19, 52, 58]. Moreover, choosing optimal values for regularization in these approaches is a significant concern because inadequate settings may cause minor perturbations in the dataset, resulting in neurophysiologically implausible outcomes [26].

In recent years, there has been rapid development of deep learning neural network (DNN) techniques in various fields, including computer vision, natural language processing, image generation, and biomedical signal and image analysis [17, 12, 32, 38, 7, 22]. In the context of

source imaging, DNNs based on the end-to-end approach treat the mapping of the EEG signal to source activity as a black box, which can be optimized by the parameters of the network without relying on prior knowledge of the physical characteristics of the head [28]. However, most existing DNN methods for EEG source imaging (ESI) assume that the probability distributions of training and testing samples are independent and identically distributed (i.i.d.), which is difficult to meet in practice. The probability distribution of EEG signals and source signals can change due to various factors such as the patient's mood, illness, and physiological state, leading to a violation of the i.i.d. assumption and resulting in the domain shift problem. Remarkably, to the best of our knowledge, there has been no research on the domain shift problem in ESI, which hinders the potential and applicability of deep neural networks in addressing ESI challenges.

In light of the limitations of conventional EEG source imaging techniques, as previously outlined, including susceptibility to noise, domain shift instabilities, and the complexity of selecting appropriate regularization values, we propose a novel method called denoising autoencoder-based unsupervised domain adaptation (DAE-UDA) to address these challenges. The UDA component in our method aims to narrow the distribution gap and learn common features from labeled training data in the source domain and unlabeled test data in the target domain. Furthermore, to address the challenge of low signal-to-noise ratio (SNR) and noise in EEG signals, we drew inspiration from previous related work and proposed an effective architecture based on the denoising autoencoder (DAE) [56] to remove the noise in EEG signals. Through the collaborative efforts of the encoder and decoder in DAE, our model is capable of removing noise from EEG signals and extracting relevant features, thereby improving the robustness and stability of the model in the presence of noisy EEG signals. To the best of our knowledge, we are the first to utilize an unsupervised domain adaptation approach (UDA) to mitigate the issue of domain shift in ESI.

1.2 Thesis Outline

The rest of this thesis is organized as follows. Chapter 2 introduce the background, significance, challenges in the EEG source imaging problem and the related work of ESI and domain

adaptation. In Chapter 3, we give the details and problem setup of domain adaptation problem on ESI we need to solve with. Chapter 4 introduces the details of the forward model and the simulated process used to simulate EEG and source activity data. Moreover, the architecture and details of DAE-UDA algorithm we proposed are shown in Chapter 4. Chapter 5 uses the simulated data and real data to evaluate the performance of DAE-UDA and compares DAE-UDA with some classical existing ESI methods. Chapter 6 discusses and concludes the findings of the study.

Chapter 2

Background

2.1 Electrophysiological Source Imaging (ESI) Problem

2.1.1 Background and Definitions of ESI Problem

Electroencephalogram(EEG) are important technologies for measuring human brain activity and physiological state, which have an advantage over other non-invasive tools, higher temporal resolution and a cheaper cost of measurement than other techniques like functional magnetic resonance imaging (fMRI). The advantages of EEG and flexible application make EEG become one of the most used methods in brain biology and human neurology. With the increase in the number of patients with epilepsy and other brain diseases and the development of brain science, many researchers realize that there is a need for effective methods to study the activity of nerves in the brain. More and more researchers are starting to study brain activity by using invasive tools and non-invasive methods. EEG which includes spatial and temporal information generated by the underlying brain electrical activity is one of the most important method of non-invasive source imaging methods in recent years [35][47][42] [27][20].

The process of generating the external surface potentials or magnetic fields from a definite setting of neuronal current activities in the brain is called the forward problem of EEG. In contrast, the EEG inverse problem is the process of reconstructing brain activity sources from external measurements of signals in the scalp, which is called the electromagnetic source imaging (ESI), also known as electromagnetic source localization (ESL), problem. However,

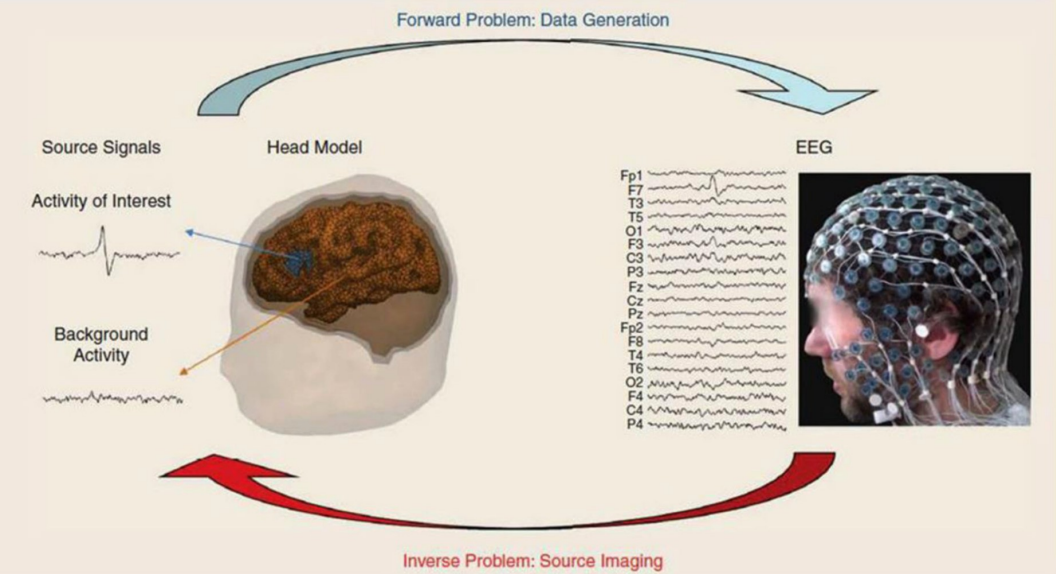

Figure 2.1: An illustration of forward and inverse problems in the context of EEG[3]

such scalp topographical maps like EEG are influenced by the volume conduction effect, which causes us only to get a rough estimation of the underlying sources. Therefore, electrophysiological source imaging (ESI) was created and developed to greatly enhance the spatial and temporal resolution of EEG signals. ESI is a inverse process of predicting the underlying electrical activity in subject's brain and scalp from the recording EEG signals and aims to search a brain source distributions which can fit the recorded EEG signals [27]. In essence, the ESI is a non-invasive prediction of brain underlying activity which based on the projections to the sensors on the scalp and constitutes an inverse advantage.

2.1.2 Importance and Significance of ESI Problem

The related researches in EEG source localization shows that EEG source localization techniques are important and effective in the diagnosis and treatment of many brain abnormalities and diseases. In the past, it has been a great challenge to find the source of brain diseases in the brains of patients like epileptics or ADHD patients. The EEG source localization techniques have more achievements and contributions in Epilepsy and Attention Deficit and Hyperactivity Disorder (ADHD) among the brain diseases which have been studied by the ESI methods. Thus, in the following, the contributions and significance of ESI techniques in epilepsy,

ADHD, and other brain abnormalities will be introduced separately. First, we will review the ESI methods used in detecting epilepsy spikes. In addition, we will study the application of ESI in ADHD.

Diagnosis of ADHD Abnormalities Using BSI Based on EEG Signal

Attention deficit and hyperactivity disorder called ADHD is a serious and common brain disease that is usually found in children. Associated medical researchers consider ADHD as a clinical psychiatric condition that will influence frontal circuitry with respect to deficits in practical cognitive functions [2]. According to related studies, ADHD is a disorder that happened in patients' childhood and rarely continues into adulthood [29]. Moreover, some other studies have shown that there is a delay in patients with ADHD [39][51]. ADHD patients will face many challenges and difficulties in daily life and work like high living costs, interpersonal relationship, and harmful academic and work consequences. In addition, patients with ADHD also suffer an altered level of inattention, hyperactivity, and violence. Therefore, it is very significant and necessary to find a method to find the source of the disease in the brain of the ADHD patient.

The brain source localization which is based on the abnormal EEG signals of ADHD patients shows a new way to help doctors diagnose ADHD, find the source of the disease and treat ADHD. Some papers has shown that the application of the parents' EEG signals can help to evaluate the impact of pharmacological and non-pharmacological treatments on electrocortical activity [2][29]. Moreover,some researches investigate using the combining of high quality EEG signals based source localization application in find if the ADHD-subtype specific modulations of neurophysiological processes are different for different type of ADHD patients or not and distinguishing them. These studies have shown that ESI methods and techniques can help associated medical researchers and physicians diagnose and treat ADHD abnormalities in patients with brain disease.

Detecting and Localizing Epileptic Seizures by Using ESI

Traditional methods used to detect and treat epilepsy are always invasive and harmful to epileptic patients. For example, doctors usually use subdural electrode method to localize the position

of epileptogenic tissue. However, due to the invasive nature of the technique, this method likely causes infections in the brain and scalp of patients.Thus, it is very necessary and useful for the epilepic patients to find a non-invasive method without risk of infection to localize the localization of epileptogenic tissue. Recently, brain source localization based on EEG signals from patients has become a novel and non-invasive method with great potential for development to help detect and localize epileptic seizures. Many researchers have investigated the application of ESI at the epilepsy site since 1995 [55][37][31][44][11][53]. These studies investigate many aspects of how to use ESI techniques in epileptic seizures, such as the relationship between the number of sensors and the precision of epileptogenic tissue localization, the restrictions that can restrict the prediction space and solve the ill-posed problem. Fig. 2.2 shows the result investigated from one of the related studies that investigates the relationship between source location and electrode number in pediatric patients with partial epilepsy based on the inverse solution of sLORETA. In Fig. 2.2, the blue dot shows the maximum localization, and the yellow line presents the resection boundaries. This paper concludes that the accuracy of the predicted location of the source of abnormal EEG signals will be improved when the number of electrode and sensor increases. However, this result and improvement are not obvious or significant for a number of electrodes larger than 128 [53].

In addition to the above results and applications, brain source localization based on EEG signals has other advantages and good points in comparison to traditional inverse source localization methods. Although invasive methods are more effective and more precise, they cause invasive damage to the patient's brain, affect normal brain function, interfere with patient recovery, and are very expensive in practice. Compared to invasive methods, the non-invasive method of ESI has great advantages in cost, patient friendliness, operability, etc. Using the ESI methods, we can predict the source activities by only using EEG signals that are recorded by the non-invasive methods on the head of patient. Furthermore, ESI helps physicians and researchers narrow the gap between EEG recordings and generators on the brain nerve. Once we have obtained the correct detail information on the source activities such as locations, intensity, extents, and polarity, we can efficiently, accurately and quickly find the pathogenic location of patients with epilepsy and take measures to control the development of the disease[34]. Moreover, dealing with the ESI problem using the noninvasive method can help researchers and

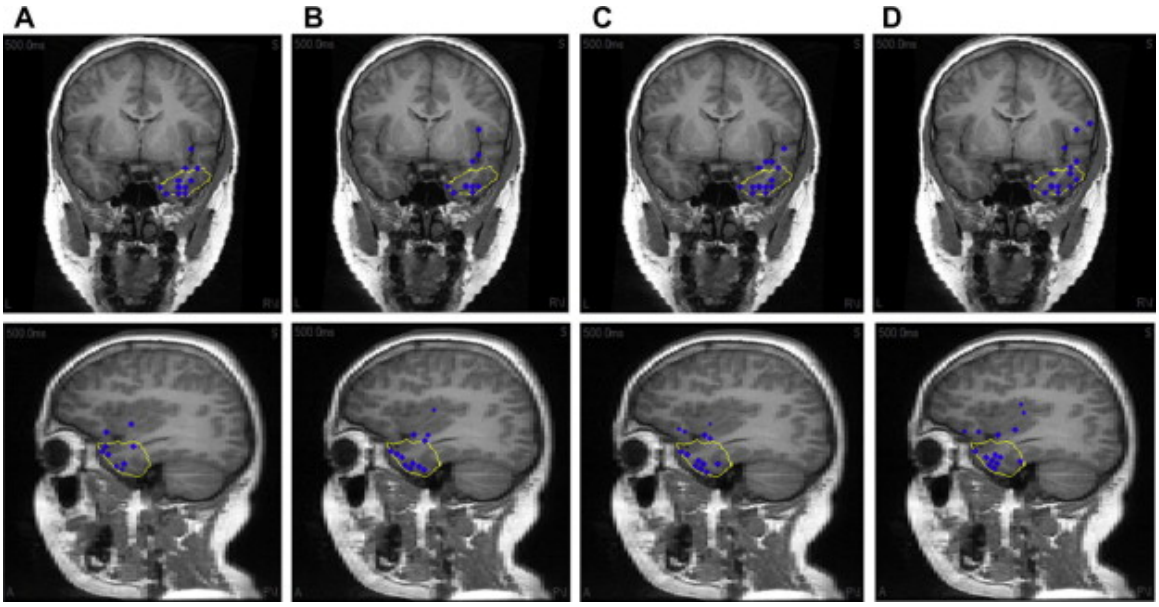

Figure 2.2: Relationship between the number of electrodes and the location of the source of the interictal spike in patients[53]

scientists better understand the information and details about different functional areas of the brain in a cheaper and safer way.

2.1.3 Difficulties and Challenges we are facing in ESI Problem

The Ill-posed Challenge of ESI Problem:

Although, the non-invasive method has more advantages than other methods, we still face some difficult and important challenges, which seriously affect the implementation and need to be solved at first. The most important and toughest problem we need to deal with is that the ESI problem is a highly ill-posed inverse problem, which means that there are infinite theoretically reasonable and possible solutions for a recorded and given measured EEG signals. The reason why the ESI problem is highly ill-posed is that the number of sensors or channels of external measurements like EEG is limited and not enough compared with the number of unidentified source dipoles, which becomes a long-standing challenge for the ESI problem.

The Prior Knowledge Impacts on The Accuracy of ESI Problem

Moreover, the classical ESI methods need to assume some prior information about the characteristic and physiological status of the subject's brain to create the head model for prediction. The accuracy of the prior information will significantly impact the performance and prediction error of the model. Furthermore, prior information about source activity is achieved by constraints that are often adopted to enable mathematical tractability but may not accurately reflect actual source configurations [50]. Thus, the accuracy of regression of the ESI problem strongly depends on the prior information and the forward model capabilities to accurately simulate the head anatomy of the head of subject from the recorded data and available structural data like MRI, fMRI, etc. Many statistical and deep learning approaches have been proposed to deal with these problem and to find the correct source dipoles. Some of them enhance the head model within the individual-specific forward model, using the head geometry complexity of the head tissue compartments and the prior information of the head morphology. Some researchers validate the proposed methodology using 25 subjects, from which a set of magnetic-resonance imaging scans is acquired, extracting the anatomical priors and an electroencephalography signal set needed for validating the ESI scenarios. The results obtained confirm that the incorporation of patient-specific head models enhances the accuracy performed and improves the localization of focal and deep sources [8]. In next section, we will introduce some classical and famous statistical and deep learning methods in ESI problem to illustrate relevant achievements, progress and existing problems.

2.2 Related work

In this section, we will introduce the background and related work in the ESI problem and the domain adaptation problem. According to recent related research, almost one third (38%) papers solves the inverse problem by statistical method [2] and many researchers used the ANN to deal with the ESI problem. Thus, we separate the ESI approaches into two parts. The first one is classical and statistical approaches that proposed in the early research period and the second part is the deep learning approaches which are proposed in recently years and show great future in this yield. The traditional and statistical methods usually used for EEG source imaging

are centered on the optimization or probabilistic framework where regularization techniques or pieces of prior information are exploited to constrain the solution space. The deep learning methods always treat the inverse process of ESI problem as a black box and train the neural network like CNN or ANN to simulate the black box to deal with the ESI problem without prior information. At the last of this section, we introduce some related work and background in the transfer learning and domain adaptation, which are useful in narrowing the domain shift in ESI problem.

2.2.1 The Related Work Solving ESI Problem by Statistical Methods

For the ESI problem, the one kind of popular brain source localization methods is statistical method, which accounted for thirty percent of all ESI methods in recent years[2]. Statistical methods for ESI can be mainly classified into different categories, including statistical methods based on minimum norm estimate (MNE), recursive multiple signal classification method (MUSIC), beamformer localization method and other statistical methods. These statistical methods will be introduced below.

Smooth Solution Methods Based on MNE and Related Methods

The minimum norm estimate (MNE) approach [57] is a typical smooth solution method. The MNE applies the L_2-norm regularization to constrain the source space to deal with the ill-posed problem of brain source localization and predict spatially smooth sources. Although the results predicted by MNE and variant methods are good in the aspects of current resolution and estimation, these methods cannot address the problem of deep source activity in the outermost cortex. The reason is that the solution of MNE methods is a harmonic function, which attain maximum values at the outermost cortex in this case.

Due to the disadvantages of MNE, some researches propose some new methods, such as weighted minimum norm estimate solution (wMNE) and low-resolution electromagnetic tomography (LORETA) to get lower error of localization distance and to predict well in the position of non-boundary sources [47]. Weighted minimum norm estimate (wMNE) [15] is a variant of MNE. wMNE try to mitigate the bias towards superficial sources by adding addi-

tional weights to the sources. Low-Resolution Electromagnetic Tomography (LORETA) [46] is an improved version of wMNE method that adds Laplacian constraint and its variants are famous proponents of the MNE family that belongs to L_2 norm-based approaches. The LORETA and its variants assume that the current density of souce activity in any position of cortex is similar to the average current density of its adjacent points, which become the basis of LORETA method and force sources to be smoothly distributed through the spatial Laplacian operator. Compared to MNE and wMNE, the results of LORETA are smoother and have a lower localization error for the deep source activity. However, LORETA also have some shortcoming and disadvantage, such as low spatial resolution of prediction and blurred localized images [59]. As a variant of LORETA, standardized LORETA (sLORETA) [48] is based on the assumption of standardization of current density [2]. Exact LORETA (eLORETA) is another variant of LORETA, which focus on how to reduce the localization mistakes of deeper source. The localization accuracy of the sLORETA and eLORETA methods is better than that of LORETA, but their spatial resolution is not appropriate [2]. What's more, the L_2-norm-based approaches may produce some overly diffuse estimates for focal sources [21].

To address this limitation of LORETA and related methods, the Focal Underdetermined System Solution (FOCUSS) [18] is proposed by researchers. FOCUSS is a high resolution non-parametric technique that uses a forward model that assigns a current to each element within a predetermined reconstruction region. In this algorithm, the weights are iterated at each step from the solution of the previous step. Weighted minimum norm method is applied for mathematical calculations in the recursive steps. It is reported that the FOCUSS algorithm has better localization accuracy compared with other methods and can manage non-uniquely defined localized energy sources as well as having acceptable spatial resolution. Furthermore, it is robust against non-uniquely defined localized energy sources. The result of FOCUSS on a complex source configuration is shown in Fig. 2.3. Another famous approach is Dynamic Statistical Parametric Mapping (dSPM) [14]. dSPM combines structural and functional MRI with magnetoencephalography (MEG) to obtain spatial-temporal maps of human brain activity with millisecond temporal resolution.

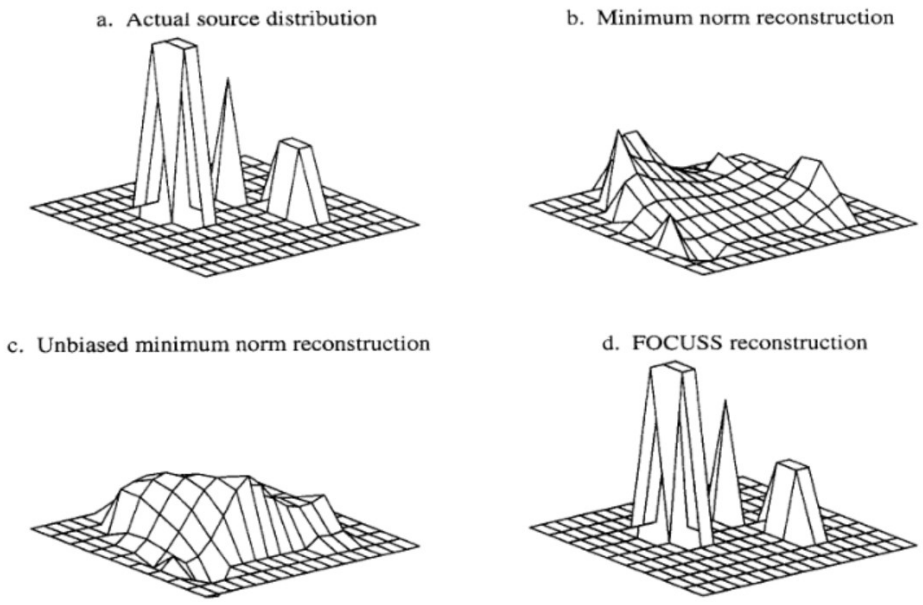

Figure 2.3: The results of reconstruction of a complex source configuration of FOCUSS and compared methods [18]

Multiple Signal Classification Algorithm (MUSIC) and Related Methods

The recursive multiple signal classification algorithm (MUSIC) was first proposed in 1995.v This algorithm tries to scan a single activity dipole through a grid confined to the subject's head or a source volume. MUSIC uses the EEG signal to produce a signal subspace and project the dipoles at each grid point from the forward model to the subspace. The location where the mapping is best fit onto the signal subspace is the location of source activity. However, MUSIC still faces some challenges and problems in the practical case. Because it is so much noise and many disturbances in practical applications that the signal subspace and forward model of patient have to include some noise and error, which impact the selection of the best mapping location in MUSIC seriously.

In 2011, Birot proposed a new generalization of MUSIC called spatially-extended neocortical sources MUSIC approach (ExSo-MUSIC approach) [4]. This method uses the higher order statistics to obtain a better result that has better robustness and can resist the Guassian noise in the modeling errors and spatial coherence. Compared with classical MUSIC methods, ExSo-MUSIC has better performance and robustness. Moreover, some researchers also pro-

posed other generalizations of MUSIC, such as recursively applied and projected multiple signal classification (RAP-MUSIC), Truncated RAP-MUSCI (TRAP-MUSIC) and blind source separation (BSS), etc. These methods use addition information, constrains or processing stage to obtain a better result and be more valid and appropriate for ESI applications.

Although these inverse algorithms have shown to, not only find the location but also estimate the correct size of sources, they can not get satisfied performance when the EEG signal has a low-level SNR or cannot overcome differences in EEG signal distribution over time. Thus, some researchers propose some novel approaches based on artificial networks or deep learning networks.

2.2.2 Deep Learning Approaches in ESI Problem and Inverse Solutions

As mentioned above, existing classical or statistical EEG source analysis methods attempt to solve the ESI inverse problem in a straight-forward manner that use different forms of prior assumptions and regularization to constrain the source space of the optimization problem. However, it is extremely difficult to find correct prior assumptions or regularization which can reflect the actual source configurations. In the aspect of deep learning, prior assumptions and regularization are more likely to be related to the parameters of an artificial neural network. Mathematically, the inverse process of the ESI problem is similar to the black box, which could be approximated by a designed deep learning network structure. Thus, some researchers tried to apply ANNs, such as convolution neural network (CNN), long short-term memory network (LSTM), to solve the inverse problem of EEG based on single or several dipoles [1]. Up to now, some achievements have been made in the application of ANNs in brain source localization of recorded EEG signals

Huang[30] proposed a new approach based on the autoencoder network and is called the Data Synthesis-Based Denoising Autoencoder (DST-DAE). The data-synthesized deep learning strategy of DST-DAE has been shown in Fig. 2.4. This paper proposed a ANNs method called DST-DAE which used an autoencoder network that has convolutional layers to encode EEG signals and deconvolutional layers to decode ESI and EEG signals to remove noise in the environment and the recording process from the noisy EEG signals. The neural network

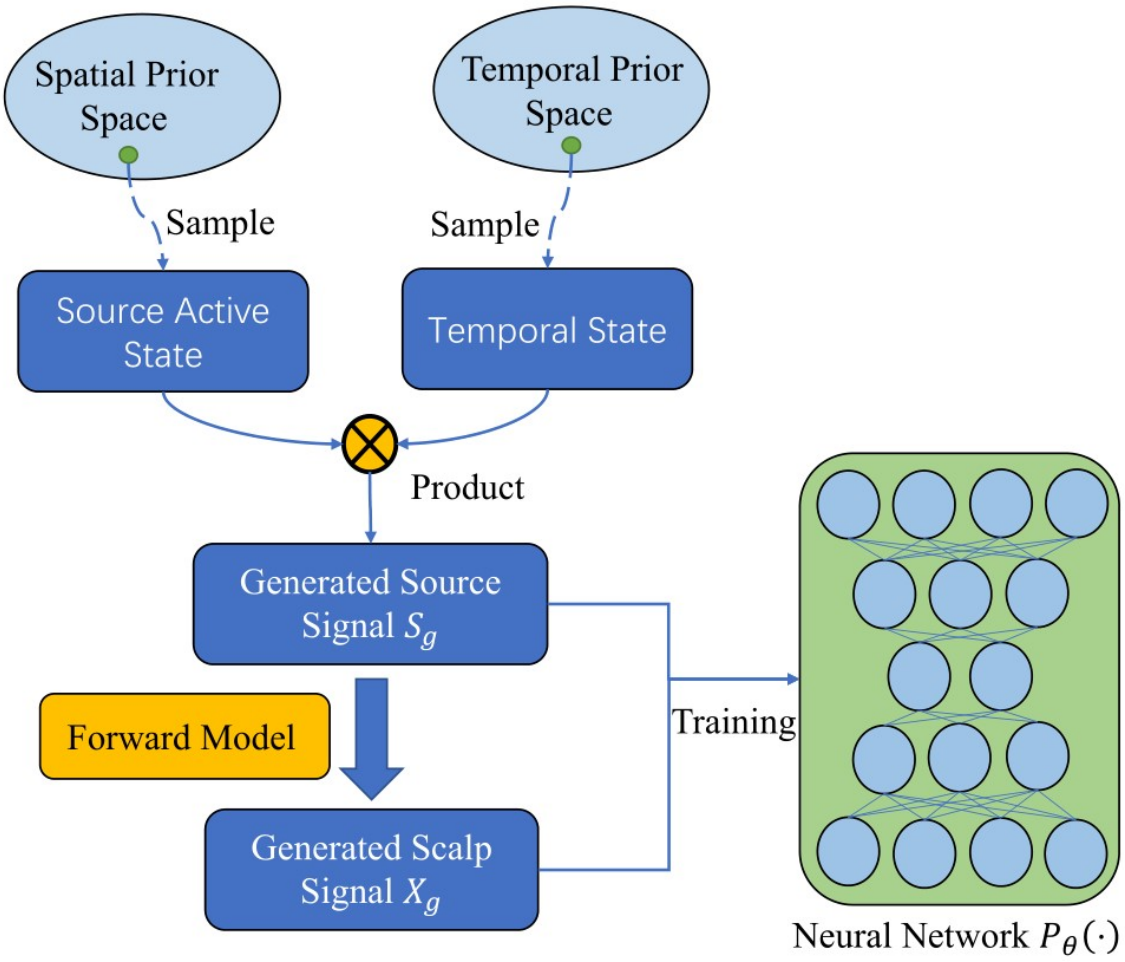

Figure 2.4: One of Data-synthesized deep learning strategy for ESI problem [30]

reformulates the brain source localization problem as a supervised machine learning problem and in This architecture achieved a reliable estimate of both the source positions and their sizes at varying levels of noise, but required a fixed-size temporal dimension of the EEG signals, which was set to 40-time slices. Furthermore, the DST-DAE was only used for single- and two-source patches and did not investigate the performance on multiple sources.

Cui [13] proposed a long short-term memory (LSTM) network to deal with the ESI problem. This network was trained on the simulated EEG data and aimed to find the localization and direction of single-dipole sources. Because the type of input and output of the model are all spatio-temporal and have same length, this model can be considered as a sequence-to-sequence (seq2seq) model. The architecture of the proposed method in this paper is shown in Fig. 2.5. However, the simulation process in this paper was a vast simplification that could not reflect the

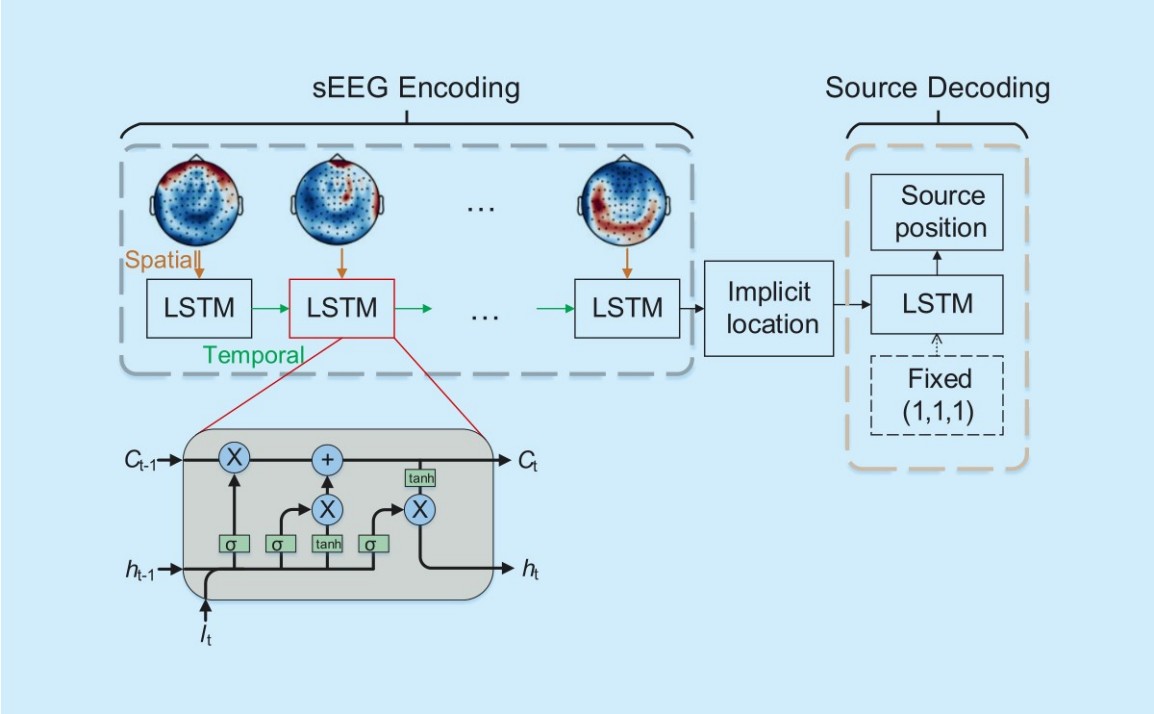

Figure 2.5: LSTM network architecture for the EEG inverse localization problem [13]

real EEG activity and the LSTM model only focused on the single dipole sources, which was an oversimplification of realistic brain activity patterns. Thus, the results and achievements in this paper can be only considered as a preliminary proof and attempt of the feasibility of the LSTM model to solve the ESI problem.

2.2.3 Unsupervised Domain Adaptation

Recently, the deep learning and artificial neural networks have achieved great achievements in many fields and enjoyed great success in various aspects of application. The most supervised deep learning methods are built on a basic and common assumption: the training and testing data are sampled from the same distribution, which we call an independent and identical distribution. However, when the training and test distributions are distinct, the classifier or regressor that is trained on the source dataset will easily suffer a decrease in performance on the target dataset, which is caused by the difference between the domains called domain shift [49] or domain shift. Furthermore, in some cases, the dataset we used to predict or classify don't have enough or even any labeled samples. We only have some related but differently

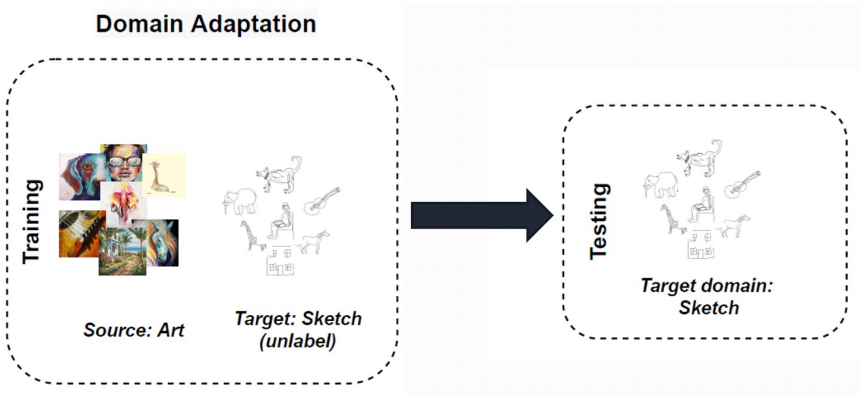

Figure 2.6: An example of unsupervised domain adaptation

distributed labeled to train our model. Therefore, unsupervised domain adaptation (UDA) has been proposed to handle domain shift, knowledge transfer, and unsupervised learning. Unsupervised domain adaptation (UDA) is the task of training a statistical model on labeled data from a source domain to achieve better performance on data from a target domain, with access to only unlabeled data in the target domain [43].

The domain-adversarial neural network (DANN) is a famous and classical work in UDA, which first introduced the idea of adversarial training into UDA [16]. The main thought of DANN is using the adversarial architecture in a two-player game to confuse a domain discriminator and to learn the transferable feature representations. The architecture of DANN is illustrated in Fig. 2.7. However, DANN was designed for learning transferable representations in the classification problem and much unnecessary domain related information and features is involved. Thus, the generalization to the regression problem in the target domain is impacted.

Zhang proposed a new measurement called Margin Disparity Discrepancy to overcome and bridge the gap between the theory and algorithm existed in adversarial learning of UDA [60]. This paper define a novel divergence MDD for domain adaptation and give the exact generalization bounds that uncover reveal the trade-off between generalization error and the choice of margin. This method and divergence can be transformed into some adversarial learning methods for unsupervised domain adaptation. Thus, we are inspired by these idea and MDD discrepancy to proposed a new algorithm based on MDD to overcome the domain shift in ESI problem and bridge the gap between the samples in the source domain and the samples in the target domain.

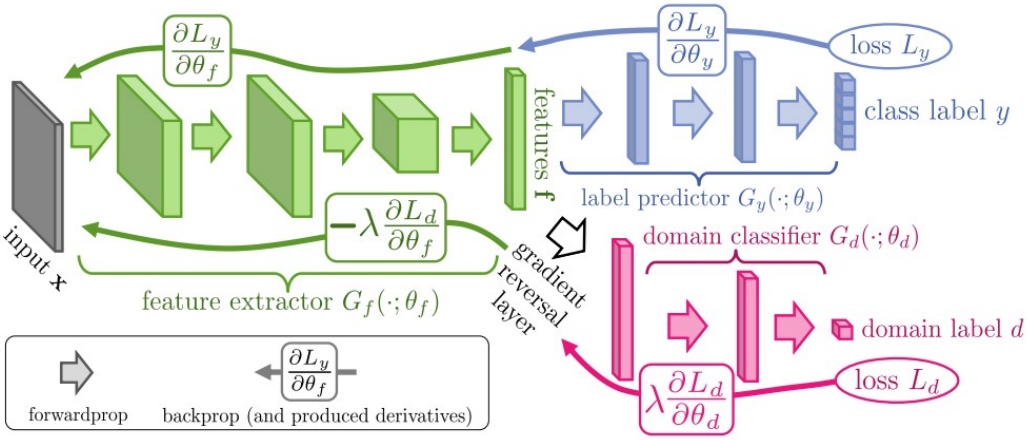

Figure 2.7: The architecture of domain-adversarial training of neural networks [16]

Chapter 3

Unsupervised domain adaptation problem on EEG source imaging

In this section, we introduce the ESI problem and related definitions for the domain adaptation in ESI problem. We first give a brief introduction of the forward problem about ESI, then the ESI domain adaptation problem is denoted. Next, we give the goal we want to achieve in the ESI domain adaptation problem.

3.1 Forward Problem of ESI

The forward problem in EEG source imaging involves the computation of the EEG signal on the scalp from the distribution of brain source activity through the use of the lead field matrix. This matrix represents the electric current field generated within the volume conductor of the head [40]. The lead field matrix is a critical tool in simulating EEG data and obtaining the corresponding source labels. Since it is difficult to obtain the corresponding source signal non-invasively in real-life scenarios, the simulation of EEG and source activity signals through the lead field matrix of the forward problem is crucial in the training of deep neural networks. The relationship between the source signal and the corresponding EEG signal can be mathematically expressed as a linear model:

$$c = Hs \tag{3.1}$$

where $c \in \boldsymbol{R}^{n\times 1}$ is the generated clean EEG signal from n electrodes on the scalp, which doesn't include any noise. $H \in \boldsymbol{R}^{n\times m}$ is the lead field matrix that reflects the relationship between the neural activity of the source of the m dipoles in the brain and the EEG activity on the scalp, and $s \in \boldsymbol{R}^{m\times 1}$ represents the neural activity of the source signal in m dipoles. In practical applications, EEG signals are often mixed with many noises, which often come from eye movement signals, muscle electrical signals, power grid interference, etc. To make the simulated EEG signal more realistic, we artificially add noise to the EEG signal, which can be expressed as:

$$e = Hs + \varepsilon \tag{3.2}$$

where $e \in \boldsymbol{R}^{n\times 1}$ is the noisy EEG signal with artificial noise, and $\varepsilon \in \boldsymbol{R}^{n\times 1}$ is the artificial noise which is similar to the noise in real EEG signal.

The lead field matrix is the linear mapping between the scalp potential measured by the electrodes and the brain source signal. The forward problem relies on the establishment of the lead field matrix. In practice, the lead field matrix$\boldsymbol{H}$ is computed by solving Maxwell's equations using for example a boundary element methods (BEM) [36], based on structural MRI scans of specific subjects or an average classical lead field template. Once the lead field matrix is determined, the forward problem can be solved.

Compared with forward problem, ESI is the inverse process of the forward problem, requiring the computation of the brain source activity distribution from the EEG signal collected on the scalp of a subject.

3.2 Unsupervised Domain Adaptation Problem in ESI

In the unsupervised domain adaptation problem, we have a labeled dataset from the source domain and an unlabeled dataset from the target domain. The distributions of samples in these two datasets are different, which causes the domain shift problem. Learning a discriminative classifier or regressor in the presence of a domain shift between two different distributions is known as domain adaptation [16].

In the unsupervised domain adaptation problem in ESI, we also have the source domain $\mathcal{S}$, and the target domain $\mathcal{T}$. For the source domain $\mathcal{S}$, we can draw a label source dataset, which

can be expressed as:

$$D_S = \{(e_i^S, s_i^S)\}_{i=1}^{N_S} \in \mathcal{S} \tag{3.3}$$

where D_S is the labeled dataset drawn from the source domain $\mathcal{S}$, and e_i^S represents the i-th noisy EEG signal in dataset, and s_i^S is the corresponding i -th source signal for the EEG signal e_i^S, and N_S indicates the number of samples in source dataset D_S.

For the target domain $\mathcal{T}$, we can also draw an unlabeled dataset, which can be expressed as:

$$D_T = \{e_j^T\}_{j=1}^{N_T} \in \mathcal{T} \tag{3.4}$$

where D_T is the unlabeled dataset drawn from the target domain $\mathcal{T}$, and e_j^T is the j-th noisy EEG signal, and N_T indicates the number of samples in D_T. During training, the examples in D_T are unlabeled, and we cannot use the corresponding source signal s_j^T to optimize our model.

In the ESI domain adaptation problem, we try to solve a domain shift problem caused by the same patient's different sessions or emotional instability, signal acquisition conditions change. Since the physiological properties of the same patient's head do not change easily over a period of time, we can assume that the leading matrix is invariant in the two datasets. Change in the patient's emotion, signal acquisition conditions, and sessions will only influence the distribution of EEG signal and source signal and cause the domain shift. Our goal is to train a regressor F that uses the given knowledge of D_S and D_T and to obtain good performance on prediction of the source signal of the unlabeled samples from D_T.

Chapter 4

Method

In this section, we first give a brief introduction about the lead field matrix, simulation method and the forward model that we used in the data simulation. Second, the denoising autoencoder technique is explained. Then we show the architecture and loss functions of the denoising autoencoder-based unsupervised domain adaptation network (DAE-UDA) for domain shift problem in ESI.

4.1 Lead Field Matrix and Simulation

The DAE-UDA network is utilized to address the ill-posed ESI problem by treating it as a regression problem. To successfully overcome the domain shift between the source and target datasets, model need to learn common features and uncover the mapping function using a nonlinear artificial neural network. To achieve this goal, sufficient samples from both the source and target datasets are required for network training. However, direct recordings of electrical activity in subjects' brains are invasive, which makes it difficult to acquire enough source data samples in practice. Therefore, we need deal with a forward problem that computes the EEG signal on the scalp from the brain source activity distribution by the specific lead field matrix of a real head model. In the forward problem, we utilize a data synthesis approach based on real lead field matrix that combines spatio-compactness and the properties of a realistic subject's head model.

The lead field matrix is a crucial component in the simulation of the EEG signal and source

activation. It provides a solution to the forward problem and enables the creation of a generative model. In order to produce realistic simulated EEG data, we utilized the standard sample data from the MNE package, which includes actual EEG signals and a related lead field matrix built from MRI data of a real subject. This dataset was acquired at the Athinoula A. Martinos Center of Biomedical Imaging of the MGH/HMS/MIT, using the Neuromag Vectorview system. The original MRI data set was obtained using an MPRAGE sequence with a Siemens 1.5 T Sonata scanner. Our forward model employed a source space with $p = 7498$ dipoles along the cortical surface provided by Freesurfer tool. These dipoles were selectively activated to simulate brain activity in the subject. We used a set of 60 EEG electrodes, with all problematic channels removed to mitigate signal disturbance.

In this section, the simulation of EEG and source signal was carried out using the method described in the related research [28]. To ensure the authenticity of the simulation data, five parameters were taken into account during the simulation process: the number of activated source dipoles, the extent of the activated area, the intensity amplitude of the activated dipoles, the distribution of the activated area and the signal-to-noise ratio (SNR). Each simulation sample included at least one activated dipole cluster, with the number of activated clusters increasing to five in some simulation settings. These activated clusters can be considered smooth areas of activation within the brain. The center of the activated cluster was generated by selecting an activated dipole randomly from our cortical source model and growing the dipoles in the surrounding region using the approach described in [9]. Our growing method involved recursively activating all surrounding adjacent dipoles starting from the central activated dipole to generate a larger source extent based on the distance from the center. Each center dipole had a dipole moment, which were referred to as amplitudes of the activated dipole. The moments of neighboring dipoles decreased based on the distance from the center activated dipole, following the classical Gaussian distribution we set for the distribution shape. Moreover, the mean of the Gaussian distribution was the moment of the center dipole, and its standard deviation was half the radius of the dipole clusters, which enabled the generation of a smooth activated source area.

After generating the source signal, we can compute the corresponding EEG signal on the scalp by the lead field matrix in Eq. 3.1. However, these generated EEG signals are not as

noisy as the actual EEG signals. Therefore, to generate more realistic EEG for training, we use the Gaussian noise generation method described in [54] to add noise ε to the simulated EEG data based on the real SNR of realistic EEG signals of subjects. Specifically, we analyze the realistic data in the MNE sample dataset firstly and calculate the SNR of the EEG signal to get the level of noise in practice. According to our analysis, the SNR of the EEG signals in sample dataset is about 4.5 dB. Second, we create Gaussian noise based on the SNR level of realistic signals and add the noise to the simulated EEG signals.

According to the above process, we change the setting of the parameters of the simulation process to imitate the domain shift and obtain the source dataset D_S and target dataset D_T. In the source dataset D_S, we have $N_S = 10000$ labeled examples $(C^S, E^S, S^S) = \{(c_i^S, e_i^S, s_i^S)\}_{i=1}^{N_S}$, which include the simulated source signal S^S and the clean EEG signal C^S without artificial Gaussian noise and the noisy EEG signal E^S that has been added artificial Gaussian noise ϵ^S. In the target dataset D_T, we have the $N_T = 10000$ unlabeled examples $(E^T) = \{e_j^T\}_{j=1}^{N_T}$, which includes noisy EEG signal E^T with the artificial noise ϵ^T. In training of models, C^S, E^S, S^S and E^T can be used for training, but source signal for target samples S^T, ϵ^S, and ϵ^T are invisible during training.

4.2 The Design of DAE-UDA Network

The traditional approaches, which are typically used to address the ESI problem, may potentially overfit the noise in EEG signals, resulting from factors such as eye movement, power frequency interference, and ambient electromagnetic interference. Moreover, the change of distribution of source and EEG signal causes the domain shift problem and seriously impacts the model's performance and robustness. As far as we know, no relevant researchers or papers study the domain shift problem in ESI, which limits the potential application and prospects of artificial neural networks to address this problem.

To overcome above problems and challenges, we propose a more anti-interference and robust model that integrates unsupervised domain adaptation, latent-space learning, and discriminative representation into the framework of the DAE-UDA. Inspired by the work on regression domain adaptation [60], EEG encoding-decoding networks, and recent neural networks on the

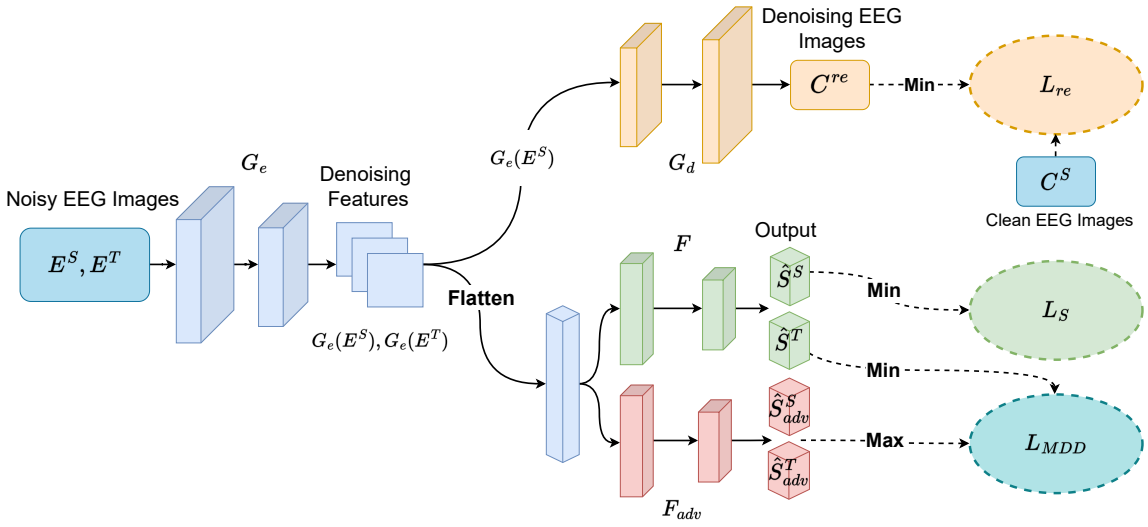

Figure 4.1: Overall architecture of the proposed DAE-UDA method. The arrows represent the input-to-output sequence of the DAE-UDA. The dashed arrows and lines indicate the output and corresponding loss functions.

ESI problem, we use the blocks in the denoising autoencoder with the spatio stepwise convolution and deconvolution tailored to EEG signals to extract robust features from the noisy EEG signal from the latent space features in the denoising autoencoder. These features can capture underlying correlations and spatio structure, which could be used effectively to remove noise from signals and to reconstruct signals without noise. Moreover, we apply the adversarial idea to the domain adaptation problem. By constructing two regressors with the same structure to fight against each other, we conduct a minimax game to narrow the difference in data distribution between the two datasets and achieve model generalization.

The overall architecture of network is illustrated in Fig. 4.1. The architecture of our model can be separated into two components: the denoising auto-encoder is used to remove noise from signals and another part for domain adaptation to overcome the domain shift. The two parts are introduced and presented separately.

4.2.1 Overall of DAE-UDA

The input of DAE-UDA is the labeled examples in the source domain D_S and unlabeled examples in the target domain D_T. Note that all EEG signals in the two datasets have been

interpolated into the 9*9 EEG images that can be used in the convolutional neural network and then fed into the neural network as samples for training. Thus, all the following EEG signals and related notation refer to the interpolated EEG images. This method converts the EEG signal into an EEG image according to the position of the EEG electrode on the scalp and the intensity of the corresponding collected electrical signal. The position of the pixel in the image represents the positional relationship of the EEG electrode, and the value of the pixel corresponds to the intensity of the EEG electrical signal.

In training, the DAE encoder layers G_e map the noise EEG images to the latent space and try to extract the noise-free features first. The outputs of G_e are the noise-free features $G_e(E^S)$ from the source domain and denoising features $G_e(E^T)$ from the target domain. After the DAE encoder layers G_e, $G_e(E^S)$ will be fed into the decoder layers G_d. $G_e(E^S)$ and $G_e(E^T)$ will be fed into the regressors F and F_{adv} for domain adaptation separately according to different domains of samples. Finally, the decoder G_d will output the denoising cleaned EEG images, the regressors will predict the source activated label of source domain's features and the target domain's features, which will be used for network optimization and loss computation.

4.2.2 Denoising Autoencoder

To remove the noise in the EEG signal, we proposed a denoising architecture, which is based on auto-encoder technique and illustrated in Fig. 4.2. In denoising process, we only used the labeled samples E^S from the source dataset D_S to simulate a situation where clean EEG signal is scarce in the target dataset due to the poor acquisition environment and other reasons. First, we feed the noisy EEG images in the source dataset to Encoder G_e to extract denoising features $G_e(E^S)$. The decoder layers are consisted by two convolution layers to extract features from samples and dropout layers to overcome the overfitting problem.

For the DAE decoder layers G_d, the denoising features $G_e(E^S)$ extracted from the labeled samples from the source domain will be fed into these layers. In the DAE decoder layers G_d, which consists of spatial decoding blocks, batch normalization (BN) layers, and two transposed convolution layers, these layers will decode spatial information from denoising features $G_e(E^S)$ to compute and generate reconstructed denoising EEG images C^{re} as output from the

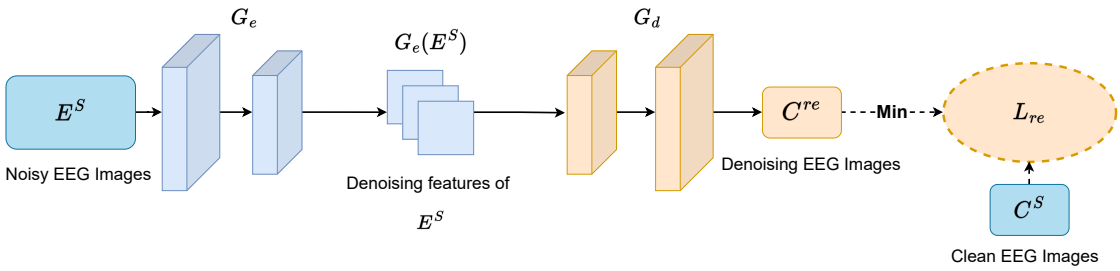

Figure 4.2: Overall architecture of denoising auto-encoder.

denoising autoencoder. The BN layers are add into the encoder and decoder layers, which will overcome the distribution and convariate shift that may happen in feature mapping and in using the large scale dataset to training. Moreover, BN layers can also make prediction not only insensitive to the initialization of the parameters of each component in the network, but also make the learning process quickly and smoothly. These reconstructed images C^{re} can be regarded as reconstructed images of the original noisy EEG images after the neural network removes the noise and extracts useful features. The loss function of the denoising autoencoder will calculate the reconstruction error between clean EEG images C^S from the source domain and the reconstructed denoising EEG images C^{re} generated from noisy EEG images E^S. The loss function of the reconstruction process is as follows:

$$\begin{aligned} \min_{G_e,G_d} L_{re}(C^S, C^{re}) &= \min_{G_e,G_d} \lambda L_1(C^S, C^{re}) + (1-\lambda) L_2(C^S, C^{re}) \\ &= \min_{G_e,G_d} \frac{\lambda}{N_s} \sum_{i}^{N_s} |c_i^S - c_i^{re}| + \frac{1-\lambda}{N_s} \sum_{i}^{N_s} (c_i^S - c_i^{re})^2 \end{aligned} \tag{4.1}$$

where N_S is the total number of samples used for training in the source domain, L_{re} is the loss function to evaluate the reconstructed error between C^{re} and E^S, and λ is the trade-off parameter between the L1-norm L_1 and L2-norm L_2, which varies in different experiments. In reconstruction loss L_{re}, we use the L1 loss and L2 loss to compute the reconstruction loss. The reasons are that the L1 loss is very sensitive to subtle differences in the predictions, and L2 loss can detect errors that are caused by higher amplitudes.

4.2.3 Margin Disparity Discrepancy Based Unsupervised Domain Adaptation

To deal with the challenge of domain shift in the ESI problem, we proposed the unsupervised regression domain adaptation model for the domain shift problem in ESI. The architecture of UDA is illustrated in Fig. 4.3. In the training of UDA component, we feed labeled samples in the source dataset and unlabeled samples in the target dataset to extract the common features and narrow the domain gap. Our method is based on the margin disparity discrepancy (MDD), which is inspired by Long's related work on the regression and classification domain adaptation [60]. MDD is a novel measurement with critical generalization upper bounds and could be very flexible for use in various domain adaptation problems [60]. According to related theories and researches about MDD, the supremum of network's error on unlabeled target samples is determined by several factors: the empirical regression error of network on the source domain, the empirical MDD loss, the ideal error and the complexity terms. In practice, the upper bound of the target error is mainly affected by the first two important factors and the latter two parameters can be ignored [60][16]. In order to get better results, our model needs to get a lower error on samples of the source domain and to narrow the empirical MDD between source dataset and target dataset. Thus, the optimization object we need to solve is a minimization problem for the optimal regressor:

$$\min L_{UDA} = \min\Big(L_S + L_{MDD}(D_S, D_T)\Big) \tag{4.2}$$

where L_S is the regression loss for the samples in the source dataset D_S and $L_{MDD}(D_S, D_T)$ is the empirical MDD loss between the source dataset and the target dataset. To achieve this object, the UDA network is divided into two parts which are called Regressor F and Adversarial Regressor F_{adv}, which have the same architectures, but the objectives of two regressions are different. For Regressor F, Regressor F first accepts the denoising features of the labeled samples $G_e(E^S)$ in the source dataset and the denoising features of the unlabeled samples $G_e(E^T)$ in the target dataset as input, then predicts the corresponding labels of the source samples $\hat{S}^S$ and the label of the target samples $\hat{S}^T$. For the source label $\hat{S}^S$, we evaluated the regression error between $\hat{S}^S$ and the ground-true label of the source samples S^S by loss L_S. For the target label S_T, we will transfer these characteristics to the adversarial regressor to calculate the

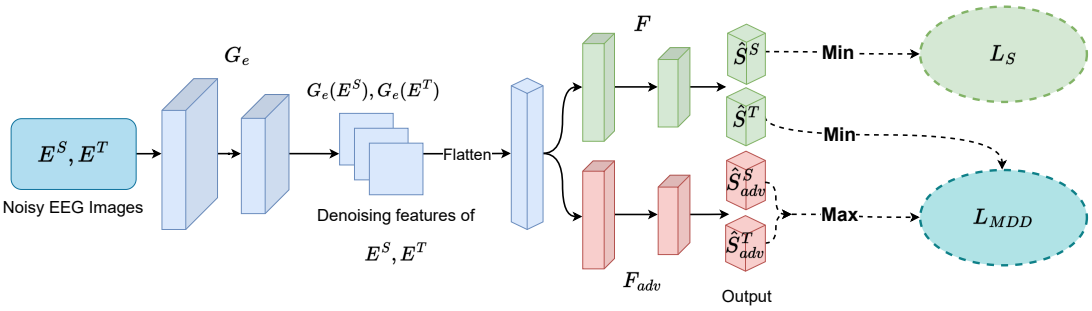

Figure 4.3: Overall architecture of UDA.

discrepancy between S_T and S'_T, which is the divergence metric between the source and target domains. The loss of regression of the samples in the source domain L_S can be expressed as:

$$\min_{G_e,F} L_S(S^S, \hat{S}^S) = \min_{G_e,F} \frac{1}{N_s} \sum_{i}^{N_s} (1 - cos(s_i^S, \hat{s}_i^S)) = \min_{G_e,F} \frac{1}{N_s} \sum_{i}^{N_s} (1 - \frac{s_i^S \cdot \hat{s}_i^S}{\|s_i^S\| \, \|\hat{s}_i^S\|}) \tag{4.3}$$

where L_S is cosine similarity which could evaluate the similarity between the true source activities S^S of the examples in the source dataset and the predicted source activities $\hat{S}^S$. The aim of L_S is to narrow the difference between prediction and ground true to decline the prediction error of regressor on source dataset.

The regressor error on the source samples can be minimized by the loss function L_S of the Regressor F. However, we still need to narrow the L_{MDD} between the source and the target dataset to reduce the supremum prediction error on the target dataset. According to related research, the minimization problem of L_{MDD} between two dataset y is a minimax game since MDD is defined as the supremum over hypothesis space, which can be quantified as the supremum of the difference between the predictions of two different regressors F and F_{adv} for features of samples from different datasets D_S and D_T. This could be expressed as follows:

$$\begin{aligned}
\min_{G_e,F} L_{MDD}(D_S, D_T) &= \min_{G_e,F} \mathrm{disp}_{G_e(E^T)}(F^*_{adv}, F) - \mathrm{disp}_{G_e(E^S)}(F^*_{adv}, F) \\
\mathrm{disp}_{G_e(E^S)}(F^*_{adv}, F) &= \frac{1}{N_S} \sum_{i}^{N_S} |F^*_{adv}(G_e(e_i^S)) - F(G_e(e_i^S))| \\
\mathrm{disp}_{G_e(E^T)}(F^*_{adv}, F) &= \frac{1}{N_T} \sum_{j}^{N_T} |F^*_{adv}(G_e(e_j^T)) - F(G_e(e_j^T))|
\end{aligned} \tag{4.4}$$

where $disp(\cdot)_{G_e(E^S)}$ and $disp(\cdot)_{G_e(E^T)}$ is margin discrepancies that evaluate the difference between the output of regressors F and F^*_{adv} on the datasets. F^*_{adv} is the optimal regressor in

hypothesis space, which maximizes the difference between the output of two regressors to approximate the supremum of the difference L_{MDD} infinitely. In practice, it is very challenging to compute the MDD between the source and target domain, because it is very difficult to find an exact regressor F^*_{adv} in the hypothesis space to compute the MDD, which means that we can only find an optimization problem to find a regressor to approximate F^*_{adv} in L_{MDD} infinitely. So in order to find such a regressor F^*_{adv}, we used the adversarial regressor F_{adv} to play a minimax game with Regressor F.

The adversarial regression F_{adv} has the same architecture and input data as the regressor F but has a different loss function and optimized object, which are very important to narrow the domain gap and to approximate F^*_{adv} infinitely. The denoising features of target samples $G_e(E^T)$ and the denoising features of source samples $G_e(E^S)$ will be fed into the Adv-Regressor F_{adv}. After processing and predicting, the Adv-Regressor F_{adv} will output the label of the target samples S'_T. To find the optimal regressor F^*_{adv}, the object of F_{adv} in the minimax game of L_{MDD} can be expressed as follows:

$$\begin{aligned} F^*_{adv} &= \operatorname*{argmax}_{F_{adv}} L_{MDD}(D_S, D_T) \\ &= \operatorname*{argmax}_{F_{adv}} \mathrm{disp}_{G_e(E^T)}(F_{adv}, F) - \mathrm{disp}_{G_e(E^S)}(F_{adv}, F) \end{aligned} \tag{4.5}$$

In training, to facilitate model training and realize the minimax game, we introduce the GRL layer [16] between the denoising features and the Adv-Regression. Therefore, the final optimal function of the UDA component can be expressed as follows:

$$\begin{aligned} \min_{G_e,F} \max_{F_{adv}} L_{UDA} &= \min_{G_e,F} \left(L_S(S^S, \hat{S}^S) + \max_{F_{adv}} L_{MDD}(D_S, D_T) \right) \\ &= \min_{G_e,F} \left(L_S(S^S, \hat{S}^S) + \max_{F_{adv}} \mathrm{disp}_{G_e(E^T)}(F_{adv}, F) - \mathrm{disp}_{G_e(E^S)}(F_{adv}, F) \right) \end{aligned} \tag{4.6}$$

4.2.4 Final Optimal Function of DAE-UDA

To sum up the above, we can give the final optimal function L of our model, which consists of three components: the reconstruction error of denoising EEG signals L_{re}, the regression error

of samples in the source domain L_S and the loss function of the Adv-Regressor L_{adv}:

$$\begin{aligned}\min_{G_e,G_d,F}\max_{F_{adv}} L &= \min_{G_e,G_d,F}\max_{F_{adv}}\Big(L_{re}(C^S,\hat{C}^S)+L_S(S^S,\hat{S}^S)+L_{MDD}(D_S,D_T)\Big)\\ &= \min_{G_e,G_d} L_{re}(C^S,\hat{C}^S)+\min_{G_e,F} L_S(S^S,\hat{S}^S)+\min_{G_e,F}\max_{F_{adv}} L_{MDD}(D_S,D_T)\end{aligned} \tag{4.7}$$

where the optimal object of G_d is to reconstruct clean denoising EEG images that are similar to real cleaned EEG signals. The feature encoder G_e attempt to remove the noise in signals and to extract domain invariant features which can be used to predict more accurately, reconstruct more completely and narrow the L_{MDD}. In the next chapter, we will introduce the details of implementation of our model. Moreover, the experimental results on simulated and real datasets and the analysis of the results will be presented in the next chapter.

Chapter 5

Experiment

In this section, we will present experiments using realistic and simulated data to demonstrate the efficacy of our model. The performance of the proposed model will be compared with some state-of-the-art algorithms, namely ConvDip [28], dSPM [14], eLORETA [45], DANN [16] and MNE [57]. Specifically, the five experiments were devised based on different simulated data and one experiment based on real EEG signals to compare the performance of our model with that of four existing classical and novel ESI methods, including three norm regularization and classical EEG source imaging approaches: minimum norm estimation (MNE) [57], eLORETA [45] and dynamic statistical parameter maps (dSPM) [14], which were proposed for the reconstruction of a spatially extended and activated source. Moreover, two deep learning neural networks, Convdip [28] and Domain-Adversarial Training of Neural Networks [16], are compared with our method. The first neural network, Convdip, were specifically designed to estimate activated source dipoles at peak time point. The second neural network, DANN, is a classical and famous domain adaptation network, which is the first to introduce the idea of adversarial architecture and Gradient Reversal Layer (GRL) into the field of domain adaptation. Most research and articles on domain adaptation [60][6][25] used DANN as a baseline model to compare and evaluate the performance of their model. Thus, the performance of DANN on the ESI problem can become a symbol and an important reference standard to measure the quality of our model. The performance of our model is investigated by evaluating the estimated source signals in a variety of experimental settings using multiple metrics, mean localization error (MLE), mean squared error (MSE), normalized mean squared error (nMSE), and area

under curve (AUC) [23]. First, we simulate different sampled datasets as the samples extracted from different domains by changing several aspects of the simulation setting (Extents, SNR, Number of activated source dipoles). Secondly, we evaluate our model and the baseline model on simulated samples to compare the performance of different methods and analyze the results. Finally, the real EEG dataset was analyzed to further illustrate the superiority of our model in practice. Note that the evaluation set is the target dataset with label whose label is invisible to all models during training.

5.1 Forward Model

The prediction of the location of source activity is based on four aspects: the EEG signals measured on the scalp, the spatial sensor position of electrodes, the head conductive property, and the location of source dipoles. In our sample dataset, there are 60 EEG channel electrode caps on the scalp and the method of subdivision of the source space is the octahedron (OCT6). The octahedron 6 divides the brain into two hemispheres, each with 4098 source dipoles per thousand square centimeters. Thus, our source space has 7498 dipoles on the white matter surface of the brain in both hemispheres. In oct6, the spacing between each dipole is 4.9mm and the surface area of per source dipole is 24 mm^2. For the last aspect of the head conductive property, the sample dataset uses structural magnetic resonance imaging (MRI) data to build subject-specific anatomical models of the scalp, inner/outer skull, and cortical surface to obtain the head models of real subjects, which are based on the classical numerical method: Boundary Element Method (BEM). The conductivity parameters of scalp, skull and cortical the dataset used are 0.3 S/m, 0.006 S/m and 0.3 S/m that are used widely for the conductivity of head [28].

5.2 Settings of Simulation Data

In the simulation data generation method we used, We divide the characteristics of the source activities in the scalp of the brain into five aspects: the number of activated source dipoles, the extents of activated area, the amplitudes of intensity of activated dipoles, the distribution

Table 5.1: Simulation parameters of various **sources numbers** for source and EEG signal

Parameters	Parameter Range	Parameter Type
Number of sources	S**: 1** T**: 2, 3, 4, 5**	**Various**
Extents	21- 58 mm	Shared
Amplitudes	1-10 nAm	Shared
Source shape	Gaussian	Shared
Signal-to-noise ratio	4.5	Shared

of source activated area, and the signal-to-noise (SNR) ratio. To simulate the domain shift of the brain situation of subjects in practice, we set up different experiments on these five aspects respectively, which could evaluate the impact of the offset of each parameter on the models' performance about handling domain shift and the transfer ability of our model. In each aspect, we will change one aspect of five aspects in an experiment to simulate each 10000 samples separately in the source and target domain to obtain the datasets with domain shift. Specifically, we will set a fixed parameter for the data in the source domain and set different parameters to simulate the samples in the target domain. We refer to relevant research and the literature to reasonably set the range of parameter setting values [28]. Since our model operates on single time instances of EEG or MEG data, we only use the signal on the peak of the EEG signal as input, which means that the duration of the EEG data is one time point.In all experiments, the attenuation of the neighboring dipole moment follows the classical Gaussian distribution.

In research and papers about the ESI problem, the number of activated source dipoles is a very important factor for source prediction and model performance. Many regression models that perform well on the single activated dipole cannot regress the source activities of multiple activated dipoles accurately, which means that the difference in number of activated sources causes a huge domain shift and decreases the robustness of most models. Thus, we change the number of activated source dipoles and set experiment about source number to investigate and compare our model's transfer ability and robustness with baseline models. The setting of simulation parameters is illustrated in Table 5.1.

Table 5.2: Simulation parameters of different **extents** for source and EEG signal

Parameters	Parameter Range	Parameter Type
Number of sources	1	Shared
Extents	S**: 20** T**: 30, 40, 50, 60 mm**	**Various**
Amplitudes	1- 10 nAm	Shared
Source shape	Gaussian	Shared
Signal-to-noise ratio	4.5	Shared

For the second experiment, we investigate the impact of different extents of source signals on the performance of the models. The simulation setting for first experiment is shown in the Table 5.2. In the simulation setting of extents, we set various extents in the range from 20mm to 60mm according to related research. For the setting of samples in the source domain, the simulation parameters are as follows: the number of activated source dipoles is single, the extent is 20mm, the amplitudes of source activity are uniformly distributed from 1 *nAm* to 10 *nAm* and the SNR ratio of the EEG signals is 4.5 dB, which is close to the SNR ratio of the real EEG signals in the standard sample dataset in the MNE package. For the samples in target domain, all parameters setting are same as the setting of source samples except the extents. The extents of target samples are set from small to large as 30mm, 40mm, 50mm and 60mm. These settings can reflect the shift of the brain activation range as the subject's brain state and emotions change due to external stimuli or diseases that we encounter in practice. In addition, this experiment can also investigate the robustness and stability of the model in this regard.

Because different patients are affected by physical state, emotion, etc., the activity intensity of the same brain stimulation has certain changes, sometimes stronger and sometimes weaker. Variations in signal strength can also affect prediction accuracy. Thus, in the third experiment, we study the impact of amplitudes of source activities on the regression of the ESI problem. The experiment can assess the model's ability to capture weak signals and process stronger brain activity. The relevant settings of the simulation parameters are shown in Table 5.3.

Due to various interference from patients and the collection environment during data collection, the collected EEG data will be mixed with different degrees of noise, resulting in very

Table 5.3: Simulation parameters of different **amplitudes** for source and EEG signal

Parameters	Parameter Range	Parameter Type
Number of sources	1	Shared
Extents	21- 58mm	Shared
Amplitudes	S**: 2** T**: 4, 6, 8, 10 nAm**	**Various**
Source shape	Gaussian	Shared
Signal-to-noise ratio	4.5	Shared

Table 5.4: Simulation parameters of different **SNR** for source and EEG signal

Parameters	Parameter Range	Parameter Type
Number of sources	1	Shared
Extents	21- 58 mm	Shared
Amplitudes	1- 10 nAm	Shared
Source shape	Gaussian	Shared
Signal-to-noise ratio	S**: 45** T**: -5, 5, 15, 25 dB**	**Various**

variable signal-to-noise ratios. Moreover, the traditional statistical model needs to artificially set the signal-to-noise ratio of the signal to train, which cannot be automated and is seriously affected by human judgment. Therefore, we set up the final experiment on the SNR of EEG signals to evaluate the impact of different levels of noise on the ESI problem. The SNR setting of parameters is shown in Table 5.4.

Area under the ROC curve (AUC): We calculated the area under the receiver operating characteristic curve (ROC-AUC) as described in [23]. First, we will normalize all dipoles in the activated clusters to unite the amplitudes between 0 and 1, which are normalized by division of the maximum. However, the positives and the negatives in the data should be the same in AUC. To achieve this requirement, we use the method described in related research [24][10] to calculate two different AUC: AUC_{far} and AUC_{close}. Two AUCs include all positive dipoles and differ in the selection of negative dipoles. AUC_{far} is a metric that captures how well an inverse solution (1) finds the sources at the correct locations and (2) avoids false positives. AUC_{close}

also captures (1) how well sources are correctly localized but also (3) how well the size was estimated. Therefore, AUC_{close} captures the dispersion of an inverse solution.The overall AUC was then calculated by taking the average of AUC_{close} and AUC_{far}.

Mean localization error (MLE): It is a very important ability to locate the center of source activity accurately or not for the inverse model. Thus, we use the mean localization error (MLE) as a metric to evaluate the inverse performance of the models, which calculate the Euclidean distance, a common measure of inverse solution accuracy, between the positions of the maximum of predicted source label and the ground truth source maximum. However, this metric is suitable only for the single source patch.

For multiple activated source dipoles, we use the procedure similar to that described in [28]. The most important thing we need to do is to identify the location of maxima the prediction and ground truth. We first chose the dipole whose amplitudes are larger than those of its neighboring dipoles, which will yield many maxima. However, there are some positive maxima called false positive maxima can not constitute an active cluster of dipoles. Thus, we get rid of these maxima whose neighboring dipoles are not sufficiently active. Moreover, we also remove the maxima that are so close to another maximum dipole. So far we have obtain a list of locations of maxima for prediction and ground truth. Then we need match the maxima in prediction and ground truth and calculate the pairwise Euclidean distances. To match the maxima, we locate the closest activated source dipole in the prediction from the maxima in the true source and calculate the MLE by averaging these minimum distances.

Mean square error (MSE): Another metric that we use is the mean square error (MSE), which is very popular in the regression problem and the inverse problem. The MSE will calculate the square error between each dipole in estimation and true source. Due to the square processing of the data in the calculation, the metric is very sensitive to the results with large amplitudes errors and can effectively control extreme values. The MSE can be expressed as follow:

$$MSE = \frac{1}{p}\sum_{i=1}^{p}(j_i - j_i')^2 \tag{5.1}$$

Normalized mean square error (nMSE): Due to the sensitivity of MSE to extreme values, we may ignore subtle differences and cannot easily calculate the entire error level of the

regression. Thus, we normalize the values of dipoles before calculating the MSE error and get the normalized mean square error (nMSE). Normalized MSE (nMSE) was calculated by normalizing both the true source vector j and the predicted source vector j' before calculating the MSE. By normalizing the vectors, we eliminate possible offsets and capture the overall differences in the patterns more closely. The nMSE can be expressed as follow:

$$nMSE = \frac{1}{p}\sum_{i=1}^{p}(\frac{j_i}{|j|_{max}} - \frac{j'_i}{|j'|_{max}})^2 \tag{5.2}$$

5.3 Experiment Results and Analysis

As we mentioned in Section 5.2, we used different settings to simulate different ESI datasets that differ in the following parameters: subjects, SNR of the signals, activated extents of source dipoles and numbers of activated source dipoles. The settings of parameters we used followed some simulation settings in [28]. Through these different simulation setting, we can simulate the distribution of brain neural activity in different states of the same patient and the brain activity of different patients under actual conditions. We evaluated our model and baseline models on these samples from different ESI data domains and analysis the results to improve the advantage of our models.

5.3.1 Experiment with Varying Number of Sources

In the realistic situation, the EEG signals will be generated by signals that originate from several regions of the brain simultaneously, which will provoke the inversion process. Moreover, it is difficult to identify the location of sources reliably, which is caused by the low spatial resolution of the EEG signals. Thus, in the first experiment, we designed the experiment and simulation setting to evaluate the performance of the models in reconstructing more difficult samples from single- and multiple-source data sets. The details of the simulated setting are given in Table 5.1. For the samples from the source domain, the number of activated source is only single-source. For the target domain, we set the number of sources as 2, 3, 4, 5 separately to simulate the situation of multiple sources. All models are trained on single-source samples

Table 5.5: Results of transfer from single-source to multiple-source datasets

Task	Model	MSE (SD) (10^{-19})	nMSE (SD)	AUC (SD) (%)	MLE (SD) (mm)
1 to 2	Convdip [28]	**2.47** (0.07)	0.022 (0.006)	80.59 (0.41)	15.35 (0.23)
	MNE [57]	3.24	0.027	70.04	21.44
	eLORETA [45]	3.25	0.070	71.47	19.72
	dSPM [14]	3.30	0.043	71.49	21.59
	DANN [16]	2.74 (0.08)	0.018 (0.003)	85.40 (0.98)	17.72 (0.77)
	DAE-UDA	2.58 (0.16)	**0.012** (0.001)	**81.13** (1.74)	**14.06** (1.03)
1 to 3	Convdip [28]	4.37 (0.89)	0.023 (0.002)	**76.85** (0.16)	18.89 (0.74)
	MNE [57]	5.45	0.030	67.52	21.85
	eLORETA [45]	5.46	0.076	68.52	21.57
	dSPM [14]	5.55	0.044	68.21	23.69
	DANN [16]	4.40 (0.05)	0.021 (0.004)	77.97 (1.06)	21.45 (0.73)
	DAE-UDA	**4.29** (0.21)	**0.012** (0.001)	76.58 (1.03)	**16.21** (0.94)
1 to 4	Convdip [28]	**5.97** (0.07)	0.024 (0.003)	70.77 (0.84)	18.46 (0.60)
	MNE [57]	6.66	0.031	63.73	22.58
	eLORETA [45]	6.68	0.077	65.05	22.22
	dSPM [14]	6.79	0.045	65.18	23.79
	DANN [16]	5.97 (0.12)	0.021 (0.002)	71.35 (1.81)	23.56 (1.40)
	DAE-UDA	6.34 (0.34)	**0.015** (0.002)	**71.76** (0.47)	**17.67** (0.54)
1 to 5	Convdip [28]	8.85 (0.44)	0.026 (0.009)	68.37 (0.76)	21.51 (0.84)
	MNE [57]	8.77	0.032	64.06	24.16
	eLORETA [45]	8.78	0.080	65.25	23.44
	dSPM [14]	8.93	0.047	65.35	24.42
	DANN [16]	8.79 (0.14)	0.021 (0.001)	69.03 (2.09)	23.73 (0.34)
	DAE-UDA	**8.19** (0.41)	**0.019** (0.002)	**69.67** (1.61)	**19.14** (1.05)

from the source domain and evaluating on multiple-source samples from the target domain which source number are 2,3,4,5. We think that this experiment can effectively evaluate the robustness and transfer ability of our model and the baseline models under the influence of the source number.The result and the aforementioned metrics are illustrated in the Table 5.5

Results on different numbers of sources: Based on the result of the number of sources in Table 5.5, we can find that the performance of all models will worsen as the number of sources increases. The reason is that the divergence between the single-source domain and the multiple-source domain will be larger when the number of sources increases, which impairs the performance of the models. However, the MDD network clearly shows improved predictive

performance with the application of domain adaptation and obtains the state-of-the-art result. All performance metrics displayed in Table 5.1 show the highest performance compared to Convdip and baseline models, which means that the domain adaptation method can learn common and robust knowledge of different numbers of sources and effectively improve predictive performance. For the MSE metric, the MDD significantly outperforms Convdip by a large margin, with an improvement of over 50% to 5% in the MSE for the numbers of different sources.

5.3.2 Experiment with Varying Extents

The second experiment focuses on the influence of varying extents of activated source on the performance of models. Due to the change of subject's emotion, state of an illness and mental state, the activated area of the dipole cluster and the number of activated Neighboring dipoles will varying, which will have impact on the localization and regression of source activity. Thus, we change the extents of the samples from the source domain and the target domain as mentioned in Section 5.2. The extent of source domain is 20mm that is more compact than the extents of the target domain, which are 30mm, 40mm, 50mm, 60mm. This experiment can evaluate the robustness and ability to handle with different extents. The result is shown in Table 5.6. Moreover, to make the results more intuitive and easy to understand, we also map the regression result on the brain cerebral cortex and visualize the prediction of models on the brain cortex in the Fig. 5.1. The illustration shows the ground truth source label in the first picture and the results of our model and baseline models are shown in the rest pictures. The range of amplitudes of the source activity is shown in the right of pictures. Negative amplitudes of signals are represented by blue, and the lighter the color, the smaller the value. And the positive amplitudes of the signals are represented by red to orange, and the lighter the red, the higher the amplitudes.

Results of different extents: We analyzed the influence of extents on the inverse solution quality using the evaluation set introduced above. Results are depicted in Table 5.6. The visualization of losses of several models has been shown in Fig. 5.2. Across source analysis methods and evaluation measures, we found a non-surprising overall pattern of worse perfor-

Table 5.6: Results of transfer from 20mm extent to larger extent datasets

Task(mm)	Model	MSE (SD) (10^{-19})	nMSE (SD)	AUC (SD) (%)	MLE (SD) (mm)
20 to 30	Convdip [28]	0.63 (0.02)	0.012 (0.0020)	94.13 (0.16)	14.79 (0.42)
	MNE [57]	0.77	0.022	72.64	20.15
	eLORETA [45]	0.78	0.060	74.20	16.40
	dSPM [14]	0.79	0.036	74.02	19.36
	DANN [16]	0.57 (0.02)	0.015 (0.0022)	90.57 (0.87)	14.99 (0.56)
	DAE-UDA	**0.41** (0.05)	**0.006** (0.0005)	**96.83** (0.13)	**12.83** (0.29)
20 to 40	Convdip [28]	1.08 (0.02)	0.011 (0.0032)	93.47 (0.19)	15.44 (0.16)
	MNE [57]	1.47	0.025	76.78	19.66
	eLORETA [45]	1.48	0.061	75.48	16.73
	dSPM [14]	1.50	0.039	74.75	19.89
	DANN [16]	1.46 (0.01)	0.015 (0.0029)	86.76(1.76)	17.91(0.66)
	DAE-UDA	**0.95** (0.001)	**0.005** (0.0005)	**95.27** (0.70)	**12.48** (0.85)
20 to 50	Convdip [28]	1.64 (0.07)	0.011 (0.0031)	91.02 (0.44)	15.68 (0.12)
	MNE [57]	2.35	0.029	70.63	24.87
	eLORETA [45]	2.38	0.065	73.07	19.80
	dSPM [14]	2.39	0.041	73.48	21.33
	DANN [16]	2.47 (0.05)	0.018 (0.0028)	75.92 (2.97)	19.55 (0.89)
	DAE-UDA	**1.55** (0.03)	**0.006** (0.0001)	**93.35** (0.52)	**13.83** (0.77)
20 to 60	Convdip [28]	**2.59** (0.04)	0.012 (0.0069)	88.89 (0.60)	17.23 (0.20)
	MNE [57]	4.20	0.033	71.22	23.50
	eLORETA [45]	4.18	0.071	73.28	20.74
	dSPM [14]	4.28	0.044	73.20	22.03
	DANN [16]	4.29 (0.04)	0.022 (0.0066)	74.13 (1.33)	19.89 (0.15)
	DAE-UDA	3.42 (0.18)	**0.009** (0.0006)	**89.27** (0.84)	**16.92** (0.30)

mance with increasing extents. We also found a clear advantage of the DAE-UDA inverse solutions compared to the baseline approaches to the inverse problems across all evaluation metrics. Especially in the two performance metrics, nMSE and AUC, we can find that the increased extents have a great impact on neural network in these two metrics. For example, as the change of extents, the AUC of the Convdip decreases from 94% to 88% quickly and the standard deviation increases from 0.16 to as high as 0.6. Compared with the results of classical methods, we can find the DANN and Convdip has some advantage in four metrics. However, our proposed method has a great performance improvement over other methods, especially in nMSE and AUC, which shows that our method has stable performance and can learn the char-

acteristics of the signal to different extents well. Moreover, we visualize the localization of the source in Fig. 5.1, which make the advantage and better performance more intuitive and easy to understand. In Fig. 5.1, the moments of activated dipoles are plotted on the white matter surface of the brain in the view of the leaf hemisphere. In Fig. 5.1 (a), the location and pattern of the ground truth source is depicted with an obvious cluster of activated dipoles in the right cortex of the right hemisphere. The various inverse solutions of regression models that try to predict the pattern of ground truth are illustrated in Fig. 5.1 (b)-(g) next to Fig. 5.1 (a). These visualization images of statistical models show that statistical models cannot locate the approximate location of the center dipole of the activated cluster precisely and the range of the amplitudes is not quite different from the target range, some even by several orders of magnitude. Moreover, we can clearly observe that the positive region and negative region are mixed together and closer to each other in Fig. 5.1 (b)-(g), which means that the statistical models are inability to accurately judge whether the source activity is positive or negative. The results of neural networks Convdip and DANN are shown in Fig. 5.1 (b) and (f). As can be observed, the neural network can correctly predict the positive source clusters, but the reconstructed sources are diffuse, where the activation is smeared in the neighboring area and yields a few spurious sources in the vicinity of the center cluster. Furthermore, the amplitudes of the reconstructed source of DANN and Convdip are weaker than the ground truth. As for DAE-UDA, the visualization in Fig. 5.1 (g), our model can yield the highly focal source location without diffusion occurs and the polarity of sources is most positive. Since the DAE-UDA can effectively learn the features of large and small extents and narrow the shift, our model can faithfully predict the spatial extent of the source clusters with accurate estimating the amplitude. Above all, we can conclude that both quantitative and qualitative results we obtained can strong demonstrate the transfer ability and robustness of our model, which compare with other baseline algorithms.

5.3.3 Experiment with Varying Amplitudes

Results of different Amplitudes: The performance of the models on the datasets with different amplitudes is shown in Table 5.7. According to the results, we can find that amplitude changes have limited impact on models' performance. In particular, the MSE of all methods

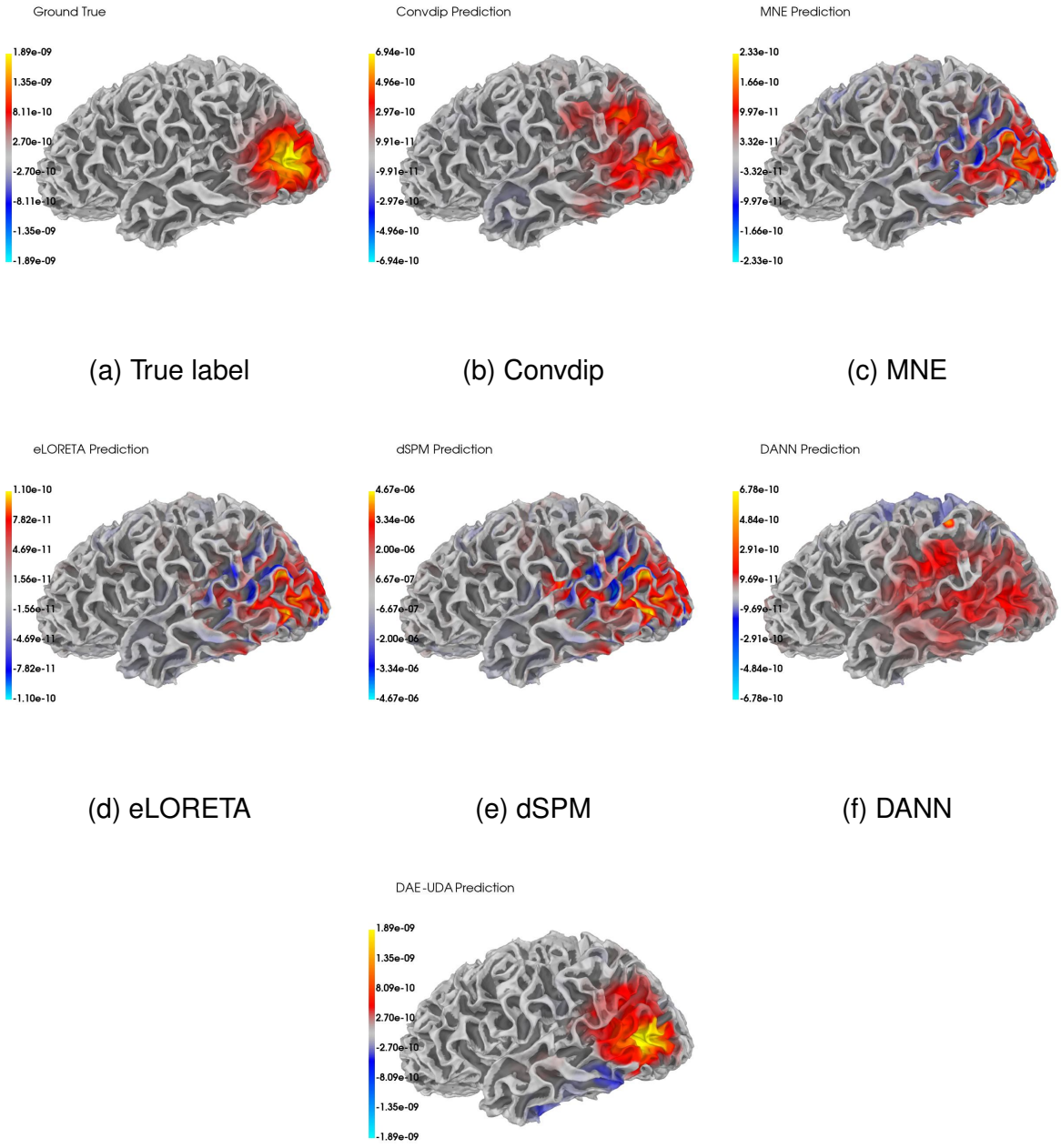

(a) True label (b) Convdip (c) MNE

(d) eLORETA (e) dSPM (f) DANN

(g) DAE-UDA

Figure 5.1: Result of models on datasets with different extents from 20mm to 60mm

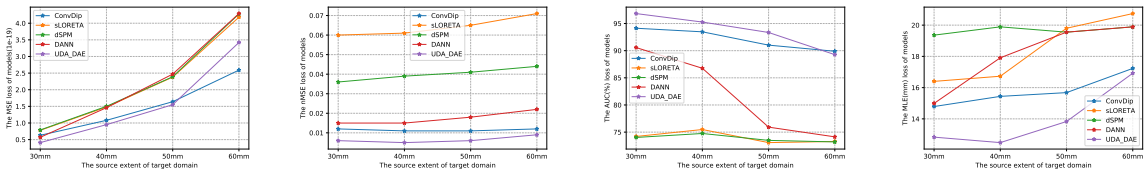

(a) MSE (b) nMSE (c) AUC (d) MLE

Figure 5.2: Losses of models from 20mm to 60mm extent.

Table 5.7: Results of transfer from 2nAm amplitude to larger amplitudes datasets

Task(nAm)	Model	MSE (SD) (10^{-19})	nMSE (SD)	AUC (SD) (%)	MLE (SD) (mm)
2 to 4	Convdip [28]	0.38 (0.01)	0.017 (0.0006)	96.31 (0.41)	13.66 (0.23)
	MNE [57]	0.74	0.026	71.95	19.52
	eLORETA [45]	0.73	0.063	74.23	16.83
	dSPM [14]	0.75	0.038	74.27	19.98
	DANN [16]	0.63 (0.14)	0.025 (0.0027)	90.31 (0.57)	16.73 (0.23)
	DAE-UDA	**0.31** (0.07)	**0.009** (0.0007)	**97.45** (0.71)	**11.85** (0.11)
2 to 6	Convdip [28]	0.90 (0.06)	0.018 (0.0008)	96.51 (0.16)	14.32 (0.19)
	MNE [57]	1.78	0.027	73.80	21.98
	eLORETA [45]	1.79	0.064	75.36	18.47
	dSPM [14]	1.82	0.039	74.98	21.13
	DANN [16]	1.39 (0.03)	0.021 (0.0002)	91.03 (0.76)	16.99 (0.41)
	DAE-UDA	**0.66** (0.02)	**0.009** (0.0007)	**97.00** (0.79)	**11.06** (0.08)
2 to 8	Convdip [28]	1.52 (0.02)	0.019 (0.0002)	95.75 (0.57)	14.68 (0.76)
	MNE [57]	2.83	0.026	73.90	21.67
	eLORETA [45]	2.84	0.063	75.09	18.32
	dSPM [14]	2.89	0.039	74.71	20.73
	DANN [16]	2.55 (0.05)	0.020 (0.0004)	91.30 (0.41)	18.41 (0.39)
	DAE-UDA	**1.15** (0.03)	**0.008** (0.0005)	**97.99** (0.46)	**10.23** (0.28)
2 to 10	Convdip [28]	2.48 (0.05)	0.018 (0.0007)	96.41 (0.59)	14.26 (0.92)
	MNE [57]	4.59	0.027	69.23	22.42
	eLORETA [45]	4.60	0.063	71.90	18.72
	dSPM [14]	4.67	0.038	72.29	21.43
	DANN [16]	3.55 (0.09)	0.024 (0.0030)	90.42 (0.19)	16.94 (0.84)
	DAE-UDA	**1.70** (0.06)	**0.009** (0.0011)	**97.40** (0.49)	**11.83** (0.67)

are sensitive to changes in amplitudes. However, the residual metrics nMSE, AUC and MLE did not change significantly. We think the reason is that the MSE metric is sensitive to the

extreme values of prediction. As the amplitude increases, the absolute error of the prediction will increase. However, the location of positive dipoles in the prediction will not change a lot, which means the metrics AUC, MLE will not be affected by the change of amplitudes. Since nMSE will first normalize the results to calculate the error, it reflects the overall error at the global level and is not sensitive to extreme errors in several dipoles. According to the result, DAE-UDA still performs better on all metrics when transferred between two different amplitudes. Especially on the nMSE, our method has excellent performance, which shows that our method is significantly better than other methods in prediction at the overall level and proves that our model is useful and meaningful in different amplitudes' ESI problems.

5.3.4 Experiment with Varying SNR of EEG Signals

Results on different SNR: The result of the transferable experiment on different SNR is shown in Table 5.4. Based on the result, we can conclude that the performance of the models is significantly affected by the SNR of the EEG signal. As the signal-to-noise ratio decreases, the performance of the models significantly degrades. The result shows that the SNR of the EEG signal is a very important factor for the localization of the EEG source. In addition, if the model needs to process EEG signals with a low signal-to-noise ratio, the performance of the model often can't meet the requirements. However, we still find that the DAE-UDA performs better than Convdip and other baseline models, although the SNRs become worse, which means that the DAE-UDA can be robust for noisy, abstract and learning useful features without noise effectively.

5.3.5 Ablation Experiment of DAE-UDA

We set different ablation experiments to give evidence that our proposed DAE-UDA model is effective and has the ability to overcome domain shift and remove noise from EEG signals in the ESI problem. Ablation is a classical method to investigate the performance of a machine learning method and discover the usefulness of the component to the whole system, which removes certain components of a machine learning system. The ablation method was proposed

Table 5.8: Results of transfer from 45 dB SNR to lower SNR datasets

Task (dB)	Model	MSE (SD) (10^{-19})	nMSE (SD)	AUC (SD)(%)	MLE (SD)(mm)
45 to -5	Convdip [28]	0.87 (0.12)	0.018 (0.005)	96.83 (0.34)	13.20 (0.49)
	MNE [57]	1.56	0.024	76.78	19.66
	eLORETA [45]	1.56	0.060	77.55	16.12
	dSPM [14]	1.59	0.039	76.70	19.10
	DANN [16]	1.40 (0.07)	0.030 (0.006)	91.50 (0.89)	16.67 (0.63)
	DAE-UDA	**0.63** (0.14)	**0.0068** (0.002)	**97.96** (0.36)	**11.03** (0.23)
45 to 5	Convdip [28]	0.89 (0.18)	0.018 (0.004)	96.33 (0.24)	14.14 (0.31)
	MNE [57]	1.50	0.026	72.26	22.91
	eLORETA [45]	1.51	0.063	73.96	17.73
	dSPM [14]	1.53	0.038	74.02	20.38
	DANN [16]	1.18 (0.02)	0.019 (0.002)	92.11 (0.94)	17.30 (0.62)
	DAE-UDA	**0.56** (0.23)	**0.0071** (0.001)	**97.91** (0.49)	**10.92** (0.94)
45 to 15	Convdip [28]	0.88 (0.29)	0.019 (0.007)	96.66 (0.08)	14.17 (0.33)
	MNE [57]	1.47	0.025	75.86	22.96
	eLORETA [45]	1.48	0.055	76.97	17.77
	dSPM [14]	1.50	0.038	76.34	20.07
	DANN [16]	1.26 (0.05)	0.019 (0.008)	91.83 (0.74)	16.22 (0.28)
	DAE-UDA	**0.50** (0.35)	**0.0059** (0.001)	**98.02** (0.18)	**10.62** (0.39)
45 to 25	Convdip [28]	0.77 (0.21)	0.018 (0.005)	96.82 (0.13)	13.28 (0.65)
	MNE [57]	1.42	0.027	76.61	19.05
	eLORETA [45]	1.43	0.056	77.57	15.88
	dSPM [14]	1.46	0.037	76.79	19.10
	DANN [16]	1.20 (0.01)	0.021 (0.002)	91.54 (0.38)	17.64 (1.01)
	DAE-UDA	**0.46** (0.40)	**0.0066** (0.001)	**98.49** (0.99)	**10.10** (0.31)

in a tutorial on speech recognition in 1974 by Allen Newell, which has become a convenient method to evaluate artificial intelligence and its durability to damage in the construction of networks [41]. Related researchers usually use the ablation method to analyze artificial neural nets in analogy to ablative brain surgery [41].

In our ablation experiment, we divide our model to three components: the denoising component for removing noisy from EEG signals G_d, the domain adaptation component to overcome domain shift F' and the prediction component for regressing the source activities of EEG signals G_e and F. In the ablation experiment, we use the experiment setting as the same as the setting in 5.2. Specifically, we use the 20mm extents EEG signals and the corresponding

Table 5.9: Ablation result of DAE-UDA

Ablation Component	MSE (SD) (10^{-19})	nMSE (SD)	AUC (SD)(%)	MLE (SD)(mm)
DAE-UDA	**3.42** (0.18)	**0.009** (0.0006)	**89.27** (0.84)	**16.92** (0.30)
Removing **Denoising** G_d	3.77 (0.15)	0.018 (0.0011)	88.03 (0.97)	17.11 (0.31)
Removing **Domain Adaptation** F'	3.65 (0.21)	0.015 (0.0021)	87.15 (1.13)	18.32 (0.49)
Removing **Both** G_d and F'	4.01 (0.18)	0.025 (0.0032)	86.42 (0.98)	19.86 (0.78)

source activity as the samples in source domain and the EEG signals with 60mm extents as the target samples in target domain. Firstly, we remove the denoising component G_d from the architecture of DAE-UDA to evaluate the effectiveness and impact of denoising component on the EEG signals and regression. Moreover, we eliminate the domain adaptation component adv-regressor F' to investigate the impact of domain adaptation on the performance of DAE-UDA. Finally, we remove both components G_d and F' to prove the effectiveness of our model.

According to the result in Table 5.9, we can find that the performance of the model without the denoising component G_d has a noticeable decrease in MSE and nMSE, which means that the noisy signal in the EEG signal has an obvious negative impact on the error of the prediction of the source activity at the entire level and some extreme peak values. Moreover, the domain adaptation component F' can obviously affect the mean localization error and AUC, indicating that domain adaptation can effectively narrow the domain shift between the source domain and the target domain. Finally, the result of model without denoising and domain adaptation components reaffirms our above viewpoints and conclusions.

5.3.6 Experiment with Real EEG Data

In the end of the experiment, we use the real EEG signal from the MNE standard dataset to evaluate the performance and robustness of our model in the real situation. This dataset was collected with the Neuromag Vectorview system by Martinos center Biomedical Imaging, which has 60 EEG channels in the collection system. During the experiments, checkerboard patterns were presented to several subjects and a smiley face was presented at the center of the visual field in each 750ms. These subjects were asked to press a key with the right index finger as soon as possible after the appearance of the smiley face.

In our experiment on the real data, we chose the peak time point (0.1s) of the recorded EEG signal of one subject in the dataset who receives specific visual and auditory stimuli and makes corresponding actions. This subject's EEG signals has been processed by low-pass filter (0-40 Hz) to remove high-frequency noise in the dataset. We evaluate the baseline models and the training DAE-UDA model, which obtained in extend experiments, on the real EEG signals to investigate the performance of our model. The results are illustrated in the Fig. 5.3.

According to related research[33], the regions of left brain activation corresponding to the subjects' responses in the experiment have been marked with circles. When subjects accepted the stimulation by eyes and moved their fingers, marked part of left brain was activated which was used to control the right hand and to do visual reaction of the subject. The region in the right back and the front of the left brain represent the activity about vision, body movement. As can be observed, the results of classical methods in Fig.5.3 (b) to (d) are diffuse in the brain and the positive and negative region are smeared in same region. DANN and Convdip in Fig.5.3 (a) and (e) yield focal sources, but can not localize the corresponding area. DAE-UDA in Fig. 5.3 (f) can successfully recover source activities in right area.

Another important observation in real EEG data is the inter-individual variability, which is a direct result of individual brain anatomies. For DAE-UDA application to the real EEG data, particularly with group data, it is thus advised to collect anatomical MRI brain scans of each individual subject. Individual neural networks then need to be trained based on each subjects' specific anatomy provided by the MRI data, which may help to achieve accurate group study source estimations. However, it raises the problem of computation time, since training individual neural networks is time consuming. A solution for it is the inter-individual transfer learning approach, where DAE-UDA is trained in one subject's anatomy and fine-tuned for each additional subject with new training data of the individual anatomies. Fine tuning could be achieved by replacing the output-layer, lowering the learning rate and retraining for only few epochs. Training time per second is another important topic, when we consider CNNs to handle the inverse problem.

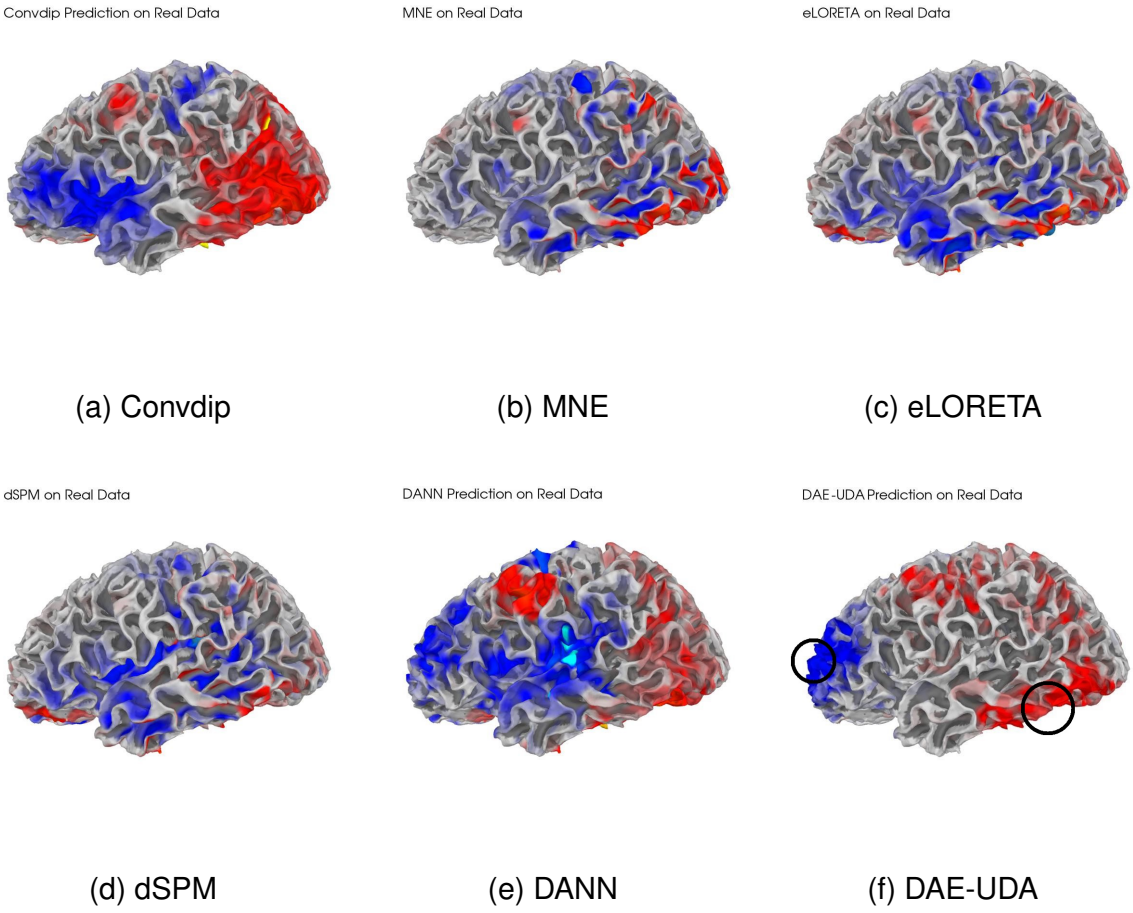

(a) Convdip (b) MNE (c) eLORETA

(d) dSPM (e) DANN (f) DAE-UDA

Figure 5.3: Result of models on real EEG signal

Chapter 6

Discussion and Conclusions

6.1 Conclusions

With the development of medicine and technology, more and more people are paying attention to finding the source of the disease of many abnormalities in the brain. The brain source localization method as one of the most important method in finding the source of brain disease have make many achievements brain disease diagnosis and treatment. The brain source localization based on EEG signals has become the main method in BSI in recent years. Many algorithms based on statistical or deep learning methods have been proposed to deal with the ESI problem. However, the noise in the EEG signals, the ill-posed feature of the ESI problem, and the domain shift between the training and testing data still impact the performance and application of the EEG methods.

In this thesis, we proposed a new EEG neural network DAE-UDA based on autoencoder and unsupervised domain adaptation to deal with these challenges in ESI problem. In our model, we use the autoencoder architecture to remove the noise in EEG signals, use the artificial neural network to consider the inverse process of ESI problem as a black box that can be approximated by a deep learning network. Moreover, based on the related unsupervised domain adaptation theory, we proposed a UDA architecture to extract the common features from the labeled samples from source domain and unlabeled samples from target domain and narrow the distribution gap. With our experiment, we 1) evaluate our methods on simulated EEG signals with different SNR level and prove the stability of our model to the low SNR signals, 2)

demonstrate the robustness and generalization of our model on the domain shift of EEG signals by changing three aspects of source activity to simulate the domain shift in practise and evaluating our model, 3) show that it can be effective and useful to deal with the ill-posed problem and avoid the influence of prior knowledge error by considering the inverse process as a black box and training the neural network to automatically learn the sensor-to-source mapping.

6.2 Applications

The domain adaptation EEG source imaging or localization based on neural networks has various applications in practice. The ability of DAE-UDA to overcome the domain shift of EEG and source activity can save the time and economic cost of extensive retraining of the model on strange patients. Moreover, the robustness of our model on low SNR EEG signals can make our model widely used to predict source activity for some low quality EEG signal.

6.3 Future Research

To predict the source activity rapidly and widely use ESI model in different actual scenarios, there are still some problems need to be solved. First, it is necessary to reduce the volume of the model and increase the response speed of the model to realize the real-time processing and prediction of the EEG signal in the actual application. Second, according to our study, We found that the divergence between the forward models of different patients was too huge to make it difficult to construct a single effective model or method to solve the ESI problems of different patients. Thus, it is a meaningful and important research direction about how to overcome the divergence between different subjects and generalize the model on them.

Bibliography

[1] Udantha R Abeyratne, G Zhang, and P Saratchandran. EEG source localization: a comparative study of classical and neural network methods. *International journal of neural systems*, 11(04):349–359, 2001.

[2] Shiva Asadzadeh, Tohid Yousefi Rezaii, Soosan Beheshti, Azra Delpak, and Saeed Meshgini. A systematic review of EEG source localization techniques and their applications on diagnosis of brain abnormalities. *Journal of Neuroscience Methods*, 339:108740, 2020.

[3] Hanna Becker, Laurent Albera, Pierre Comon, Rémi Gribonval, Fabrice Wendling, and Isabelle Merlet. Brain-source imaging: From sparse to tensor models. *IEEE Signal Processing Magazine*, 32(6):100–112, 2015.

[4] Gwénaël Birot, Laurent Albera, Fabrice Wendling, and Isabelle Merlet. Localization of extended brain sources from EEG/MEG: the ExSo-MUSIC approach. *NeuroImage*, 56(1):102–113, 2011.

[5] Joyce Chelangat Bore, Peiyang Li, Lin Jiang, Walid MA Ayedh, Chunli Chen, Dennis Joe Harmah, Dezhong Yao, Zehong Cao, and Peng Xu. A Long Short-Term Memory Network for Sparse Spatiotemporal EEG Source Imaging. *IEEE Transactions on Medical Imaging*, 40(12):3787–3800, 2021.

[6] Konstantinos Bousmalis, George Trigeorgis, Nathan Silberman, Dilip Krishnan, and Dumitru Erhan. Domain separation networks. *Advances in neural information processing systems*, 29, 2016.

[7] Erik Cambria and Bebo White. Jumping NLP curves: A review of natural language processing research. *IEEE Computational intelligence magazine*, 9(2):48–57, 2014.

[8] Yohan Céspedes-Villar, Juan David Martinez-Vargas, and Germán Castellanos-Dominguez. Influence of patient-specific head modeling on EEG source imaging. *Computational and Mathematical Methods in Medicine*, 2020, 2020.

[9] Rasheda Arman Chowdhury, Jean Marc Lina, Eliane Kobayashi, and Christophe Grova. Meg source localization of spatially extended generators of epileptic activity: comparing entropic and hierarchical bayesian approaches. *PloS one*, 8(2):e55969, 2013.

[10] Rasheda Arman Chowdhury, Jean Marc Lina, Eliane Kobayashi, and Christophe Grova. MEG source localization of spatially extended generators of epileptic activity: comparing entropic and hierarchical bayesian approaches. *PloS one*, 8(2):e55969, 2013.

[11] B Clemens, S Puskás, M Besenyei, M Emri, G Opposits, SA Kis, K Hollody, A Fogarasi, I Kondakor, K Füle, et al. EEG-LORETA endophenotypes of the common idiopathic generalized epilepsy syndromes. *Epilepsy research*, 99(3):281–292, 2012.

[12] Antonia Creswell, Tom White, Vincent Dumoulin, Kai Arulkumaran, Biswa Sengupta, and Anil A Bharath. Generative adversarial networks: An overview. *IEEE signal processing magazine*, 35(1):53–65, 2018.

[13] Song Cui, Lijuan Duan, Bei Gong, Yuanhua Qiao, Fan Xu, Juncheng Chen, and Changming Wang. EEG source localization using spatio-temporal neural network. *China Communications*, 16(7):131–143, 2019.

[14] Anders M Dale, Arthur K Liu, Bruce R Fischl, Randy L Buckner, John W Belliveau, Jeffrey D Lewine, and Eric Halgren. Dynamic statistical parametric mapping: combining fMRI and MEG for high-resolution imaging of cortical activity. *neuron*, 26(1):55–67, 2000.

[15] Anders M Dale and Martin I Sereno. Improved localizadon of cortical activity by combining EEG and MEG with MRI cortical surface reconstruction: a linear approach. *Journal of Cognitive Neuroscience*, 5(2):162–176, 1993.

[16] Yaroslav Ganin, Evgeniya Ustinova, Hana Ajakan, Pascal Germain, Hugo Larochelle, François Laviolette, Mario Marchand, and Victor Lempitsky. Domain-adversarial training of neural networks. *The journal of machine learning research*, 17(1):2096–2030, 2016.

[17] Ian Goodfellow, Jean Pouget-Abadie, Mehdi Mirza, Bing Xu, David Warde-Farley, Sherjil Ozair, Aaron Courville, and Yoshua Bengio. Generative adversarial networks. *Communications of the ACM*, 63(11):139–144, 2020.

[18] Irina F Gorodnitsky, John S George, and Bhaskar D Rao. Neuromagnetic source imaging with focuss: a recursive weighted minimum norm algorithm. *Electroencephalography and clinical Neurophysiology*, 95(4):231–251, 1995.

[19] Irina F Gorodnitsky and Bhaskar D Rao. Sparse signal reconstruction from limited data using FOCUSS: A re-weighted minimum norm algorithm. *IEEE Transactions on signal processing*, 45(3):600–616, 1997.

[20] Roberta Grech, Tracey Cassar, Joseph Muscat, Kenneth P Camilleri, Simon G Fabri, Michalis Zervakis, Petros Xanthopoulos, Vangelis Sakkalis, and Bart Vanrumste. Review on solving the inverse problem in EEG source analysis. *Journal of neuroengineering and rehabilitation*, 5(1):1–33, 2008.

[21] Roberta Grech, Tracey Cassar, Joseph Muscat, Kenneth P Camilleri, Simon G Fabri, Michalis Zervakis, Petros Xanthopoulos, Vangelis Sakkalis, and Bart Vanrumste. Review on solving the inverse problem in eeg source analysis. *Journal of neuroengineering and rehabilitation*, 5(1):1–33, 2008.

[22] George D. Greenwade. The Comprehensive Tex Archive Network (CTAN). *TUGBoat*, 14(3):342–351, 1993.

[23] Christophe Grova, Jean Daunizeau, J-M Lina, Christian G Bénar, Habib Benali, and Jean Gotman. Evaluation of EEG localization methods using realistic simulations of interictal spikes. *Neuroimage*, 29(3):734–753, 2006.

[24] Christophe Grova, Jean Daunizeau, J-M Lina, Christian G Bénar, Habib Benali, and Jean Gotman. Evaluation of EEG localization methods using realistic simulations of interictal spikes. *Neuroimage*, 29(3):734–753, 2006.

[25] Zhongyi Han, Haoliang Sun, and Yilong Yin. Learning transferable parameters for unsupervised domain adaptation. *IEEE Transactions on Image Processing*, 2022.

[26] Jens Haueisen, A Büttner, Hannes Nowak, Hartmut Brauer, and Cornelius Weiller. The influence of conductivity changes in boundary element compartments on the forward and inverse problem in electroencephalography and magnetoencephalography-Der Einfluß der Änderung der Schalenleitfähigkeit bei Randelementemodellen auf die Vorwärtsrechnung und das inverse problem in Elektroenzephalographie und Magnetoenzephalographie. 1999.

[27] Bin He, Abbas Sohrabpour, Emery Brown, and Zhongming Liu. Electrophysiological source imaging: a noninvasive window to brain dynamics. *Annual review of biomedical engineering*, 20:171, 2018.

[28] Lukas Hecker, Rebekka Rupprecht, Ludger Tebartz Van Elst, and Jürgen Kornmeier. ConvDip: A Convolutional Neural Network for Better EEG Source Imaging. *Frontiers in Neuroscience*, 15, 2021.

[29] John C Hill and Eugene P Schoener. Age-dependent decline of attention deficit hyperactivity disorder. *The American Journal of Psychiatry*, 1996.

[30] Gexin Huang, Jiawen Liang, Ke Liu, Chang Cai, ZhengHui Gu, Feifei Qi, Yuan Qing Li, Zhu Liang Yu, and Wei Wu. Electromagnetic Source Imaging via a Data-Synthesis-Based Convolutional Encoder-Decoder Network, 2020.

[31] Hiroto Iwasa, Tadahiko Shibata, Seiichiro Mine, Keijirou Koseki, Kimiko Yasuda, Yasufumi Kasagi, Motohiro Okada, Hirooki Yabe, Sunao Kaneko, and Yoshio Nakajima. Different patterns of dipole source localization in gelastic seizure with or without a sense of mirth. *Neuroscience Research*, 43(1):23–29, 2002.

[32] Anil K Jain, Jianchang Mao, and K Moidin Mohiuddin. Artificial neural networks: A tutorial. *Computer*, 29(3):31–44, 1996.

[33] Munsif Ali Jatoi, Nidal Kamel, Aamir Saeed Malik, Ibrahima Faye, and Tahamina Begum. A survey of methods used for source localization using eeg signals. *Biomedical Signal Processing and Control*, 11:42–52, 2014.

[34] Kitti Kaiboriboon, Hans O Lüders, Mehdi Hamaneh, John Turnbull, and Samden D Lhatoo. EEG source imaging in epilepsy—practicalities and pitfalls. *Nature Reviews Neurology*, 8(9):498–507, 2012.

[35] Zoltan J Koles. Trends in EEG source localization. *Electroencephalography and clinical Neurophysiology*, 106(2):127–137, 1998.

[36] Jan Kybic, Maureen Clerc, Touffic Abboud, Olivier Faugeras, Renaud Keriven, and Théodore Papadopoulo. A common formalism for the integral formulations of the forward EEG problem. *IEEE transactions on medical imaging*, 24(1):12–28, 2005.

[37] G Lantz, CM Michel, M Seeck, O Blanke, L Spinelli, G Thut, T Landis, and I Rosen. Space-oriented segmentation and 3-dimensional source reconstruction of ictal EEG patterns. *Clinical neurophysiology*, 112(4):688–697, 2001.

[38] Yann LeCun, Yoshua Bengio, and Geoffrey Hinton. Deep learning. *nature*, 521(7553):436–444, 2015.

[39] Nikos Makris, Joseph Biederman, Eve M Valera, George Bush, Jonathan Kaiser, David N Kennedy, Verne S Caviness, Stephen V Faraone, and Larry J Seidman. Cortical thinning of the attention and executive function networks in adults with attention-deficit/hyperactivity disorder. *Cerebral cortex*, 17(6):1364–1375, 2007.

[40] Jaakko Malmivuo, Veikko Suihko, and Hannu Eskola. Sensitivity distributions of EEG and MEG measurements. *IEEE Transactions on Biomedical Engineering*, 44(3):196–208, 1997.

[41] Richard Meyes, Melanie Lu, Constantin Waubert de Puiseau, and Tobias Meisen. Ablation Studies in Artificial Neural Networks. *CoRR*, abs/1901.08644, 2019.

[42] Christoph M Michel and Denis Brunet. EEG source imaging: a practical review of the analysis steps. *Frontiers in neurology*, 10:325, 2019.

[43] Timothy Miller. Simplified Neural Unsupervised Domain Adaptation. In *Proceedings of the 2019 Conference of the North American Chapter of the Association for Computational Linguistics: Human Language Technologies, Volume 1 (Long and Short Papers)*, pages 414–419, Minneapolis, Minnesota, June 2019. Association for Computational Linguistics.

[44] Megan Oliva, Stefanie Meckes-Ferber, Annie Roten, Patricia Desmond, Rodney J Hicks, and Terence J O'Brien. EEG dipole source localization of interictal spikes in non-lesional TLE with and without hippocampal sclerosis. *Epilepsy research*, 92(2-3):183–190, 2010.

[45] Roberto D Pascual-Marqui, Dietrich Lehmann, Martha Koukkou, Kieko Kochi, Peter Anderer, Bernd Saletu, Hideaki Tanaka, Koichi Hirata, E Roy John, Leslie Prichep, et al. Assessing interactions in the brain with exact low-resolution electromagnetic tomography. *Philosophical Transactions of the Royal Society A: Mathematical, Physical and Engineering Sciences*, 369(1952):3768–3784, 2011.

[46] Roberto D Pascual-Marqui, Christoph M Michel, and Dietrich Lehmann. Low resolution electromagnetic tomography: a new method for localizing electrical activity in the brain. *International Journal of psychophysiology*, 18(1):49–65, 1994.

[47] Roberto Domingo Pascual-Marqui. Review of methods for solving the EEG inverse problem. *International journal of bioelectromagnetism*, 1(1):75–86, 1999.

[48] Roberto Domingo Pascual-Marqui et al. Standardized low-resolution brain electromagnetic tomography (sLORETA): technical details. *Methods Find Exp Clin Pharmacol*, 24(Suppl D):5–12, 2002.

[49] Vishal M Patel, Raghuraman Gopalan, Ruonan Li, and Rama Chellappa. Visual domain adaptation: A survey of recent advances. *IEEE signal processing magazine*, 32(3):53–69, 2015.

[50] Grega Repovs. Dealing with noise in EEG recording and data analysis. In *Informatica Medica Slovenica*, volume 15, pages 18–25, 2010.

[51] Philip Shaw, K Eckstrand, W Sharp, J Blumenthal, JP Lerch, DEEA Greenstein, L Clasen, A Evans, J Giedd, and JL Rapoport. Attention-deficit/hyperactivity disorder is characterized by a delay in cortical maturation. *Proceedings of the national academy of sciences*, 104(49):19649–19654, 2007.

[52] C Silva, JC Maltez, E Trindade, A Arriaga, and E Ducla-Soares. Evaluation of l1 and l2 minimum norm performances on eeg localizations. *Clinical neurophysiology*, 115(7):1657–1668, 2004.

[53] Abbas Sohrabpour, Yunfeng Lu, Pongkiat Kankirawatana, Jeffrey Blount, Hyunmi Kim, and Bin He. Effect of EEG electrode number on epileptic source localization in pediatric patients. *Clinical Neurophysiology*, 126(3):472–480, 2015.

[54] Jens Timmer and M Koenig. On generating power law noise. *Astronomy and Astrophysics*, 300:707, 1995.

[55] Shinn-Yih Tseng, Fok-Ching Chong, Rong-Chi Chen, and Te-Son Kuo. Source localization of averaged and single EEG spikes using the electric dipole model. *Medical engineering & physics*, 17(1):64–70, 1995.

[56] Pascal Vincent, Hugo Larochelle, Isabelle Lajoie, Yoshua Bengio, Pierre-Antoine Manzagol, and Léon Bottou. Stacked denoising autoencoders: Learning useful representations in a deep network with a local denoising criterion. *Journal of machine learning research*, 11(12), 2010.

[57] J-Z Wang, Samuel J Williamson, and Lloyd Kaufman. Magnetic source images determined by a lead-field analysis: the unique minimum-norm least-squares estimation. *IEEE Transactions on Biomedical Engineering*, 39(7):665–675, 1992.

[58] ZhenYu Wang, Peng Xu, TieJun Liu, Yin Tian, Xu Lei, and DeZhong Yao. Robust removal of ocular artifacts by combining independent component analysis and system identification. *Biomedical Signal Processing and Control*, 10:250–259, 2014.

[59] Jun Yao and Julius PA Dewald. Evaluation of different cortical source localization methods using simulated and experimental EEG data. *Neuroimage*, 25(2):369–382, 2005.

[60] Yuchen Zhang, Tianle Liu, Mingsheng Long, and Michael Jordan. Bridging theory and algorithm for domain adaptation. In *International Conference on Machine Learning*, pages 7404–7413. PMLR, 2019.

Curriculum Vitae

Name:	Runze Li
Post-Secondary Education and Degrees:	Tianjin University Tianjin, China 2017-2021 B.SC.
Honours and Awards:	Western Graduate Research Scholarships 2021-2022
Related Work Experience:	Teaching Assistant The University of Western Ontario 2021 - 2022